Available online at www.sciencedirect.com
SCIENCE DIRECT
Geochimica et Cosmochimica Acta 70 (2006) 3149–3172
Geochimica
www.elsevier.com/locate/gca

Silica and pyroxene in IVA irons; possible formation of the IVA magma by impact melting and reduction of L-LL-chondrite materials followed by crystallization and cooling

John T. Wasson [a,b,c,*], Yoshiyuki Matsunami [a,d], Alan E. Rubin [a]

[a] Institute of Geophysics and Planetary Physics, University of California, Los Angeles, CA 90095-1567, USA
[b] Department of Earth and Space Sciences, University of California, Los Angeles, CA 90095, USA
[c] Department of Chemistry and Biochemistry, University of California, Los Angeles, CA 90095, USA
[d] Department of Earth and Planetary Sciences, Tokyo Institute of Technology, Meguro, Tokyo 152-8551, Japan

Received 7 October 2005; accepted in revised form 13 March 2006

Abstract

Group IVA is a large magmatic group of iron meteorites. The mean $\Delta^{17}O$ ($=\delta^{17}O - 0.52\cdot\delta^{18}O$) of the silicates is $\sim+1.2‰$, similar to the highest values in L chondrites and the lowest values in LL chondrites; $\delta^{18}O$ values are also in the L/LL range. This strongly suggests that IVA irons formed by melting L-LL parental material, but the mean Ni content of IVA irons (83 mg/g) is much lower than that of a presumed L-LL parent (~170 mg/g) and the low-Ca pyroxene present in two IVA meteorites is Fs13, much lower than the Fs20-29 values in L and LL chondrites. Thus, formation from L-LL precursors requires extensive addition of metallic Fe, probably produced by reduction of FeS and FeO. Group IVA also has S/Ni, Ga/Ni, and Ge/Ni ratios that are much lower than those in L-LL chondrites or any chondrite group that preserves nebular compositions, implying loss of these volatile elements during asteroidal processing. We suggest that these reduction and loss processes occurred near the surface of the asteroid during impact heating, and resulted partly from reduction by C, and partly from the thermal dissociation of FeS and FeO with loss of O and S. The hot (~1770 K) low-viscosity melt quickly moved through channels in the porous asteroid to form a core. Two members of the IVA group, São João Nepomuceno (hereafter, SJN) and Steinbach, contain moderate amounts of orthopyroxene and silica, and minor amounts of low-Ca clinopyroxene. Even though SJN formed after ~26% crystallization and Steinbach formed after ~77% crystallization of the IVA core, both could have originated within several tens of meters of the core-mantle interface if 99% of the crystallization occurred from the center outwards. Two other members of the group (Gibeon and Bishop Canyon) contain tabular tridymite, which we infer to have initially formed as veins deposited from a cooling SiO-rich vapor. The silicates were clearly introduced into IVA irons after the initial magma crystallized. Because the γ-iron crystals in SJN are typically about 5 cm across, an order of magnitude smaller than in IVA irons that do not contain massive silicates, we infer that the metal was in the γ-iron field when the silicates were injected. The SJN and Steinbach silicate compositions are near the low-Ca-pyroxene/silica eutectic compositions. We suggest that a tectonic event produced a eutectic-like liquid and injected it together with unmelted pyroxene grains into fissures in the solid metal core. Published estimates of IVA metallographic cooling rates range from 20 to 3000 K/Ma, leading to a hypothesized breakup of the core during a major impact followed by scrambling of the core and mantle debris [Haack, H., Scott, E.R.D., Love, S.G., Brearley, A. 1996. Thermal histories of IVA stony-iron and iron meteorites: evidence for asteroid fragmentation and reaccretion. *Geochim. Cosmochim. Acta* **60**, 3103–3113]. This scrambling model is physically implausible and cannot explain the strong correlation of estimated cooling rates with metal composition. Previous workers concluded that the low-Ca clinopyroxene in SJN and Steinbach formed from protopyroxene by quenching at a cooling rate of 10^{12} K/Ma, and suggested that this also supported an impact-scrambling model. This implausible spike in cooling rate by a factor of 10^{10} can be avoided if the low-Ca clinopyroxene were formed by a late shock event that converted orthopyroxene to clinopyroxene followed by minimal growth in the clinopyroxene field, probably because melt was also produced. We suggest that metallographic cooling-rate estimates (e.g., based on island taenite) giving similar values throughout the metal compositional range are more plausible, and that the IVA parent asteroid can be

* Corresponding author. Fax: +1 310 206 3051.
E-mail address: jtwasson@ucla.edu (J.T. Wasson).

0016-7037/$ - see front matter
doi:10.1016/j.gca.2006.03.023

modeled by monotonic cooling followed by a high-temperature impact event that introduced silicates into the metal and a low-temperature impact event that partially converted orthopyroxene into low-Ca clinopyroxene.

1. Introduction

Group IVA is the third largest magmatic group of iron meteorites. The metal compositions of its members indicate formation by fractional crystallization of a metallic magma, with minor superposed effects of melt trapping (Wasson and Richardson, 2001). In the magmatic groups there is a strong negative correlation between Ir and Au, with the highest Ir and lowest Au concentrations in the first crystallized solid and vice versa. Fractional crystallization requires that a magma remains well mixed, and thus implies slow cooling in an asteroidal core. Buoyancy will remove even tiny silicates (a few micrometers in size) from a molten core on a time scale orders of magnitude shorter than the time required for efficient fractional crystallization.

Silicates consisting of low-Ca pyroxene and tridymite occur in São João Nepomuceno (hereafter abbreviated SJN) and Steinbach. Tabular tridymite, seemingly deposited as veins, is present in Gibeon and Bishop Canyon. We will use the term "silica-bearing IVA irons" as a generic for these four irons, and the term "silicates" to refer to pyroxene and silica.

In Steinbach the silicates are much more abundant than the metal; in a 12-cm^2 slab, Ulff-Møller et al. (1995) observed 61.9% silicate (including 37.2% orthopyroxene, 4.5% clinopyroxene, and 20.2% tridymite), 32.4% metal and 5.7% FeS (all units are vol.%). In contrast, Scott et al. (1996) reported that silicates constitute only 19 vol.% of a large slice of SJN.

Oxygen-isotope studies show that the $\Delta^{17}O$ values in the IVA pyroxene and silica grains are about 1.2‰, similar to those in L and LL chondrites (Clayton and Mayeda, 1996; Wang et al., 2004). Figure 5 in Wang et al. (2004) shows all the data; with the exception of slightly higher values in Gibeon tridymite, $\delta^{18}O$ values are around 4–5‰, also similar to those in L and LL chondrites. This is relatively strong evidence that the IVA irons formed in an asteroid originally consisting of L- or LL-like chondrites. On the other hand, the initial Ni content of 83 mg/g (Wasson and Richardson, 2001) inferred for the IVA metallic magma is much lower than that estimated for an L-chondrite parental composition (140 mg/g; LL chondrites have Ni contents >200 mg/g; we will use a mean of 170 mg/g), although it is similar to the value of 88 mg/g expected in an H-chondrite asteroid (Ni concentrations from Kallemeyn et al., 1989; metallic Fe from least-weathered observed-fall samples of Jarosewich, 1990). These compositions indicated that the simplest model, the closed-system melting of L-chondrite parental material followed by separation of the metal into a core, cannot be correct.

Mafic silicates in a magmatic iron meteorite are expected to have formed near the core-mantle boundary of the parent asteroid. There is general agreement that the main-group pallasites (PMG) formed at a core-mantle boundary. Compositional data for PMG metal (and O-isotopic data of PMG olivine) are consistent with their formation in the same parent asteroid that produced the large magmatic IIIAB group (Clayton and Mayeda, 1996; Wasson and Choi, 2003). The silicates in pallasites consist almost exclusively of olivine; low-Ca pyroxene and phosphoran olivine are rare. Olivine is the most important mineral in most planetary and (probably) most asteroidal mantles. If a total or high-degree melt is formed in a chondritic body, the first silicate to crystallize from the melt is expected to be olivine (the enstatite chondrites constitute the only chondrite groups that may be an exception to this generalization). In olivine the (Mg + Fe)/Si ratio is about twice that in low-Ca pyroxene. Because, in chondritic matter, Mg, Fe, and Si are roughly equally abundant, the higher the fraction of iron present as FeO, the larger the normative olivine/pyroxene ratio.

As discussed in detail by Ulff-Møller et al. (1995), the fact that Steinbach and SJN contain pyroxene and silica rather than olivine is nominally inconsistent with the simple picture that they are IVA core/mantle samples from an L-chondrite or similar parent body. Either they formed from a fractionated source (favored by Ulff-Møller et al., 1995) or the chemical processes at the core-mantle site were exceptional. Special circumstances are also suggested by the observation that the FeO/(FeO + MgO) ratio in IVA pyroxene is about 0.13, much lower than the range of 0.22–0.29 observed in bulk L and LL chondrites.

The metal in 33 PMG (Wasson and Choi, 2003) shows a wide range in Ir concentrations, but most PMG have low ($0.1 < Ir \leqslant 0.32$ μg/g) to very low ($\leqslant 0.1$ μg/g) Ir contents, consistent with late formation of the metal in a fractionally crystallized core. In contrast, three of the four silica-bearing IVA irons have relatively high Ir contents. Although the IVA sample set is too small to provide adequate statistical coverage, the Ir content of the IVA metal provides an additional contrast with the PMG.

We combined a petrological investigation of SJN with equilibrium calculations and a fractional–crystallization/trapped-melt model in order to reevaluate the origin of the silica-bearing IVA irons. We address seven important questions: (a) Is it possible to form IVA irons from L-LL parental materials? (b) Why do the silicates consist of pyroxene and tridymite rather than olivine? (c) What processes caused tridymite to form veins? (d) If, as indicated by the O-isotopic data, the IVA irons originated on an L- or LL-like body, what processes caused the FeO/(FeO + MgO) ratio to be much lower than in the mafic

silicates of those chondrites, and why is the initial IVA Ni content much lower than that in L-chondrite metal? (e) Is it more plausible to form IVA meteorites from mixes of materials having different O-isotopic compositions? (f) Are the high Ir contents observed in three of the four silica-bearing IVA irons consistent with formation near a core-mantle interface? (g) Is an impact-scrambling model required for the late history of the IVA asteroid or are the observations consistent with a traditional, intact-core monotonic cooling model?

2. Samples and analytical techniques

We studied the largest available surface of the São João Nepomuceno (SJN) iron, a 9×19 cm slab from the National Museum in Rio de Janeiro (Fig. 1). We obtained and investigated two thin sections (USNM 6881-1 and 6881-5) and one thick section (USNM 6881-a) of SJN from the Smithsonian Institution (Fig. 2). We also examined a 4×4 cm slab of Steinbach (LC 755) from the UCLA collection.

The samples were examined microscopically in reflected light; the thin sections were also examined microscopically in transmitted light. The modal abundances of silicates, metallic Fe–Ni, and troilite were determined in SJN thin section 6881-5 (4988 points) and thick section 6881-a (7252 points) in reflected light using an automated point counter.

A back-scattered electron (BSE) image was made of a segment of the SJN slab (constituting ~13% of the slab's

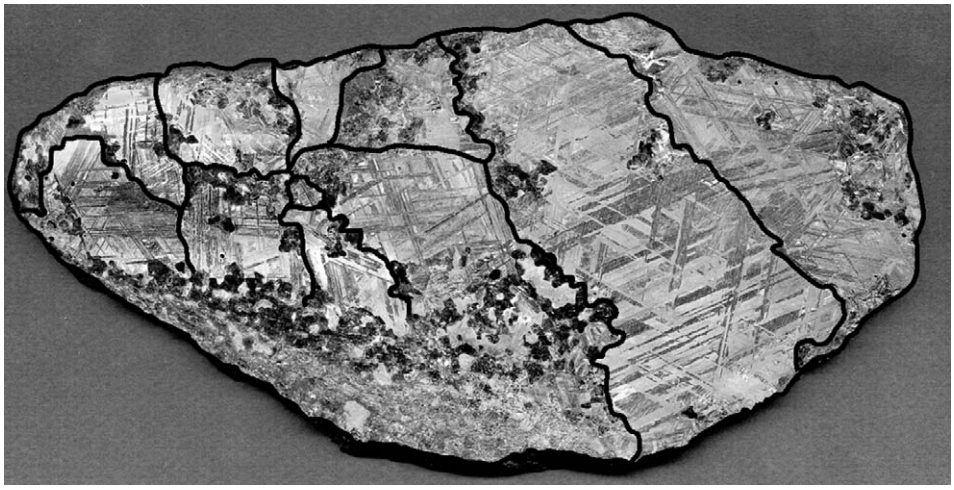

Fig. 1. Reflected light image of a large slab of São João Nepomuceno from the National Museum in Rio de Janeiro. Outlines of the primary taenite crystals are shown; the largest is 5×12 cm; all others are appreciably smaller. Massive silicates occur along the bottom of the slab (which has suffered significant oxidation). Silicates occur as massive intergrowths and as stringers. Large portions of the slab have few or no silicate inclusions.

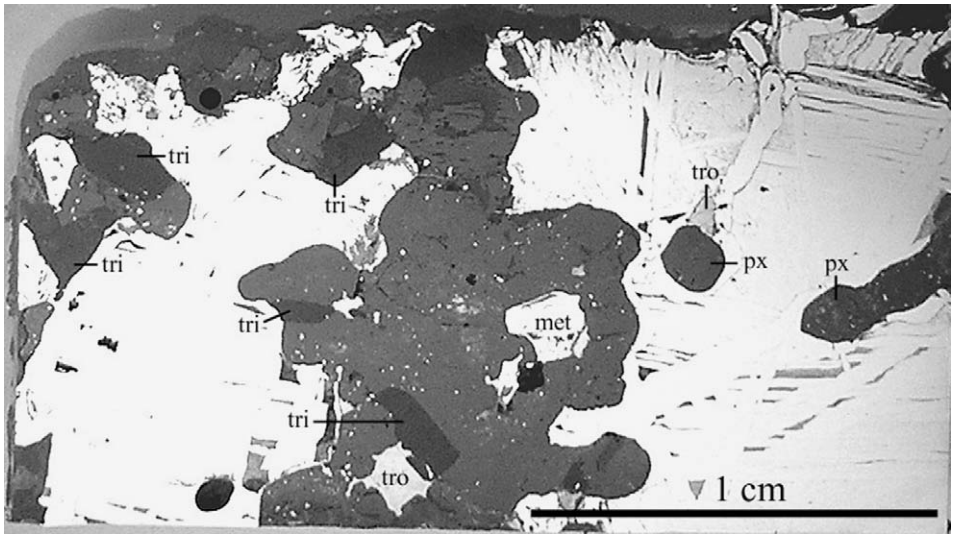

Fig. 2. Reflected light image of thick section USNM 6881-5 of São João Nepomuceno. Most silicates are low-Ca pyroxene (px, medium gray); the minor silicate tridymite (tri) is dark gray. Silicates exhibit curved boundaries with respect to metal (met, white). Small bright grains within silicates are mostly troilite with minor metal. Massive troilite (tro, light gray) is minor; it mainly occurs within the silicates and along silicate-metal boundaries.

Table 1
Modal abundances of phases in SJN and Steinbach

	SJN		Steinbach	
	vol.%	wt.%	vol.%[a]	wt.%
Metallic Fe–Ni	65.8	81.9	32.5	55.0
Troilite	4.3	3.2	6.6	6.6
Chromite	0.2	0.1	0.0	0.0
Tridymite	4.2	1.5	21.0	10.2
Orthopyroxene	23.9	12.5	38.3	27.1
Low-Ca clinopyroxene	1.6	0.8	1.6	1.1
Total	100.0	100.0	100.0	100.0

[a] Normalized mode after Scott et al. (1996) excluding 0.6 vol.% FeOOH. Although the Steinbach chromite abundance rounds off to 0.0 vol.%, the phase is present. The following mineral densities (g/cm^{-3}) were used in calculating wt.%: metallic Fe–Ni (7.9), troilite (4.67), chromite (4.7), tridymite (2.26), orthopyroxene (3.31), low-Ca clinopyroxene (3.31).

surface area) with a LEO 1430 scanning electron microscope (SEM). Silica and low-Ca pyroxene were identified with the SEM; the abundances of these phases were determined using Adobe Photoshop software.

We combined the mean silicate/troilite ratio from the SJN thin and thick section modal analyses (10.9) with the silica/pyroxene ratio from the BSE image (0.165), the orthopyroxene/clinopyroxene (opx/cpx) ratio in thin section 6881-5 (12.4), and the overall silicate/metal ratio of the slab (0.366) to determine the abundances of the individual mineral phases in the whole rock. These values appear in Table 1. Volume-percent was converted into weight percent using appropriate mineral densities. The density of low-Ca pyroxene varies with FeO content; the value used here corresponds to the composition of SJN pyroxene.

We made eight compositional zoning profiles in 1-μm steps across opx-troilite and opx-tridymite boundaries in SJN using the JEOL JXA-8200 electron microprobe at UCLA; we used natural and synthetic standards, an accelerating voltage of 15 keV, a 15-nA sample current, 20-s counting times, and ZAF corrections.

3. Mineralogy and petrology

3.1. São João Nepomuceno

Fig. 1 shows an image of the large slab of SJN. The fine-octahedrite pattern is similar to those in other low-Ni, low-Au IVA irons that are not known to contain silicates, but the sizes of the γ-iron crystals parental to the two-phase system are much smaller than those typical of normal IVA irons (mean of ~40 cm; Wasson, 1972). The boundaries are marked in Fig. 1; the largest γ-iron crystal dimension is about 10 cm, the mean size about 5 cm.

The silicates appear dark in Fig. 1 with the exception of those in an oxidized region at the bottom left. The opx and tridymite grains commonly form chains (or stringers) and irregular clusters. More massive silicate occurs along the bottom side of the slab; the outer part of this bottom region is highly oxidized, but microscopic study indicates that this region is dominated by silicates. Large portions of the slab contain few or no silicate grains. The silicate grains typically exhibit curved interfaces with metal (Fig. 2), similar to those in the subset of metamorphosed pallasites that have rounded olivine (e.g., Brenham and Springwater).

The major phases in SJN, determined by combining the modal analyses, are listed in Table 1. The silicate/metal volumetric ratio of SJN (0.45) is much less than that determined for Steinbach (1.9; Scott et al., 1996). Steinbach also has a much higher tridymite/pyroxene volumetric ratio (0.53) than SJN (0.16).

Orthopyroxene grains in SJN are typically 500–3500 μm in maximum dimension. They form sharp boundaries with other silicate grains (Fig. 3). About half of the opx grains contain 2–5 vol.% rounded to irregularly shaped opaque grains and polymineralic opaque assemblages ranging in size from 5 to 75 μm (Fig. 3a). Ninety percent of these assemblages are rich in troilite; varieties include isolated troilite grains (67%), troilite–chromite intergrowths (12%), troilite-metal intergrowths (8%) and troilite–chromite-metal intergrowths (3%). A few small tridymite inclusions are present, in many cases associated with opaques (Fig. 3a). Also present among inclusion types are isolated grains of chromite (2%) and metal (5%), and metal-chromite intergrowths (3%).

As also noted by Ulff-Møller et al. (1995), the orthopyroxene is not compositionally homogeneous. Some grains are slightly more ferroan than others: grain centers vary in composition from Fs 13.1–13.8 mol%. There is little variation in CaO (e.g., Table 2), but Cr_2O_3 varies by a factor of ~3 (i.e., 0.19–0.56 wt.%).

There is reverse zoning in orthopyroxene with respect to FeO (Figs. 4 and 5); this zoning is restricted to the outer ~10 μm of the grains where the Fs contents drop (by about 0.6 mol%) to 12.4–13.3 mol%. The zoning trends are the same at opx-troilite (Fig. 4a) and opx-tridymite (Fig. 4b) boundaries. The Cr_2O_3 content of opx co-varies with Fs, but shows appreciably more scatter; values range from ~0.20 wt.% at grain margins to ~0.35 wt.% in grain centers (Fig. 5a). The CaO (and Wo) contents show no systematic zoning trends (Fig. 5b).

We observed six low-Ca clinopyroxene grains; they range in size from 400 × 800 to 1060 × 1900 μm (Fig. 3b) and contain subparallel, somewhat wavy striations situated 30–50 μm apart. The twin lamellae appear fractured (as do those in Steinbach; Haack et al., 1996). Few opaque inclusions occur within these low-Ca clinopyroxene grains (e.g., Fig. 3b). The boundaries between the orthopyroxene and the few low-Ca clinopyroxene grains we observed in SJN are commonly subplanar or curved wherein the cpx is embayed relative to the opx.

Tridymite occurs as coarse grains (up to 1000 × 2600 μm) adjacent to low-Ca pyroxene (Fig. 3c and d) and as small inclusions (typically 10–30 μm in size) within pyroxene. (Some of the small tridymite crystals within opx grains are adjacent to small grains of troilite, metal and chromite, e.g., Fig. 3a.) In contrast to the orthopyroxene, most tridymite grains contain no completely

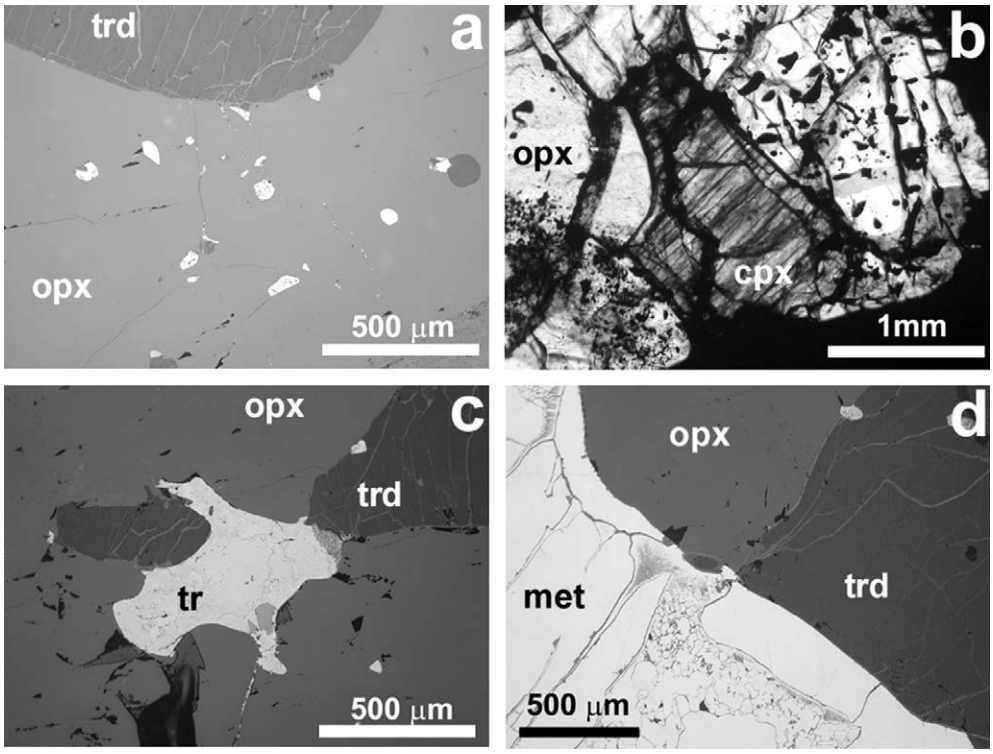

Fig. 3. Photomicrographs of silicate textures in São João Nepomuceno. (a) Numerous opaque inclusions (white) occur inside orthopyroxene (light gray), but few occur inside tridymite (dark gray, top). This suggests that the pyroxene may have formed by rapid crystallization, whereas the SiO_2 might have been deposited from a melt or vapor. (b) Low-Ca clinopyroxene grain (center with striations) occurs among inclusion-bearing opx grains. Note the much larger abundance of inclusions in the orthopyroxene. (c) Large troilite grain (white, center) inside silicate assemblage consisting of opx (light gray) and tridymite (dark gray). Note the inclusions in the orthopyroxene. The small dark patches are due to plucking during thin-section preparation. (d) Interface of silicates (gray shades) and metallic Fe–Ni (white). A discontinuous rim of swathing kamacite (white band) occurs at the interface. Thin (~2-μm-thick) veins of limonite (very light gray) occur at silicate grain boundaries; 2–6-μm-thick intersecting limonite veins occur within tridymite. (Limonite is a product of terrestrial weathering.) Images a, c, and d in reflected light; image b in plane-polarized transmitted light. opx, orthopyroxene; cpx, low-Ca clinopyroxene; trd, tridymite; met, metallic Fe–Ni; and tr, troilite.

Table 2
Selected analyses (wt.%) of orthopyroxene in SJN

Point No.	2–70	6–122	2–81	1–24	1–23
SiO_2	57.1	56.9	57.1	57.4	57.3
Cr_2O_3	0.22	0.27	0.29	0.33	0.43
FeO	8.9	8.9	9.2	9.4	9.5
MgO	34.1	33.2	33.5	33.1	33.2
CaO	0.28	0.30	0.26	0.24	0.26
Total	100.6	99.6	100.4	100.5	100.7
Fs (mol%)	12.6	13.0	13.3	13.6	13.8
Wo (mol%)	0.51	0.57	0.48	0.45	0.49

embedded opaque inclusions, although a few tridymite grains have one or two opaque inclusions at the boundary with opx (Fig. 3c and d).

There are sharp boundaries between adjacent coarse silicate grains, but in nearly every case, the boundaries are lined with ~2-μm-thick limonite rinds formed during terrestrial weathering. All of the coarse tridymite grains also contain numerous 2–6-μm-thick intersecting veins of limonite (Fig. 3a, c, and d).

Troilite grains (300–900 μm) commonly occur at metal-silicate boundaries; some large troilite grains are completely surrounded by silicate (e.g., Fig. 2). We estimate that ~80% of the troilite occurs outside of silicates and that ~20% occurs as inclusions within silicate grains. Also surrounding many of the silicate grains at the interface with metal is swathing kamacite (Fig. 3d), ranging in thickness from 50 to 300 μm.

3.2. Steinbach

The texture of Steinbach is very similar to that of SJN but the silicate/metal volumetric ratio is much higher (2.2 vs. 0.45) and Steinbach contains appreciably more tridymite (21.0% vs. 4.2 vol.% of the silicates) (Table 1). Steinbach silicates form a lacy network of 2–3-mm-thick filaments with scalloped margins intergrown with 3–4-mm-thick patches of metallic Fe–Ni. The more massive silicate and metal regions in Steinbach are both ~1 cm thick. A 1.3-mm-diameter opx spherule occurs within the metal, completely surrounded by a 30–400-μm-thick rim of swathing kamacite.

Orthopyroxene grains in Steinbach are typically 400–3500 μm in maximum dimension, similar in size to those in SJN. Some of the opx grains contain 5–15-μm-size inclusions consisting of opaque grains and polymineralic assemblages; however, the abundance of opaque inclusions in Steinbach opx is an order of magnitude lower than that

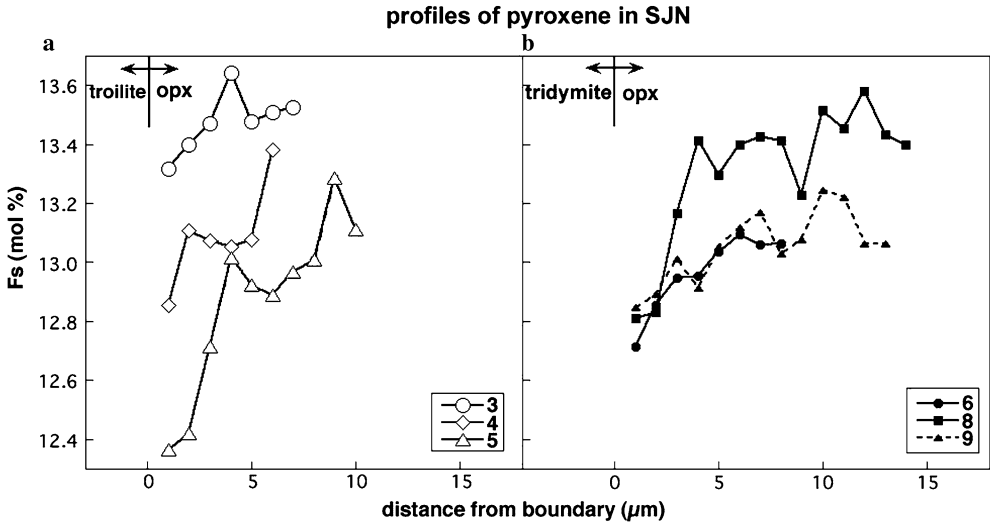

Fig. 4. Zoning profiles across the outer portions of orthopyroxene grains in São João Nepomuceno near the boundaries with (a) troilite and with (b) tridymite. Every pyroxene trace shows evidence of reduction, i.e., reverse zoning in Fs over the outer 10–15 μm of the orthopyroxene grains.

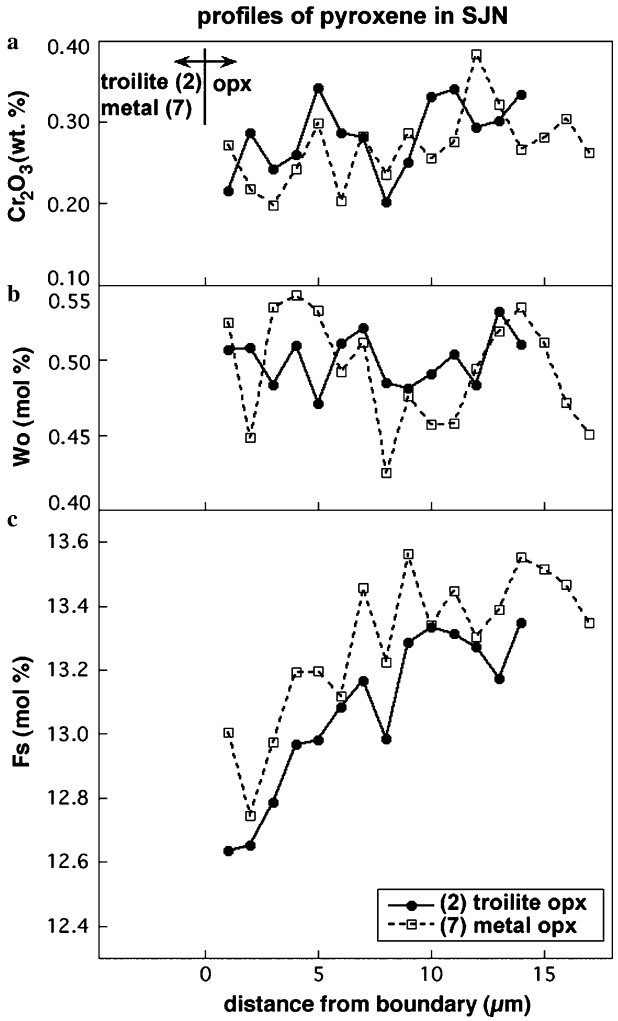

Fig. 5. Zoning profiles in orthopyroxene near the interface with troilite (trace 2) and metallic Fe–Ni (trace 7). (a) The Cr_2O_3 profile shows a weak trend. (b) The profile in Wo content shows no trend. (c) The Fs profile shows a strong reverse-zoning trend implying reduction.

in SJN opx. Nevertheless, as in SJN, most of the inclusions are rich in troilite; varieties in Steinbach include isolated troilite grains (66%), troilite-chromite intergrowths (1%), troilite-metal intergrowths (18%), and troilite–chromite-metal intergrowths (3%). Also present are monomineralic inclusions of chromite (7%) and kamacite (5%). Ulff-Møller et al. (1995) found that Steinbach pyroxene was slightly richer in FeO than that in SJN: 9.6–10.1 vs. 9.2 wt.% (i.e., Fs14 vs. Fs13).

Tridymite occurs as coarse grains (350–3000 μm in size) adjacent to low-Ca pyroxene. Most tridymite grains contain no opaque inclusions.

Troilite occurs as 1–5-mm-size grains at metal-silicate boundaries and as patches completely surrounded by silicate. Some 30–200-μm-size grains of metallic Fe–Ni also occur among the silicate grains.

Every metal patch in Steinbach has swathing kamacite along its edges. Swathing kamacite is always the first kamacite to form. This early nucleation in part explains the relative coarseness of the kamacite in this high-Ni (94 mg/g) metal.

There appear to be no large patches of metal in Steinbach. The largest metal-rich region visible on a photograph of the largest specimen (Rittersgrün, 45 × 34 cm) sent to us by A. Massauck is ~9 cm long, 1.0–1.5 cm wide, and even it contains a few silicates.

3.3. Tridymite in Gibeon and Bishop Canyon

There have been several reports of tridymite in Gibeon (e.g., Berwerth, 1902; Schaudy et al., 1972). Fig. 6a shows an apparently discontinuous 26-mm-long, 0.7–1.4-mm-wide tridymite platelet in UCLA specimen IN 590; it seems likely that it is continuous in three dimensions. As reported by Schaudy et al. (1972), the length of the plate is limited by the size of the 5-mm-thick section. These authors stated

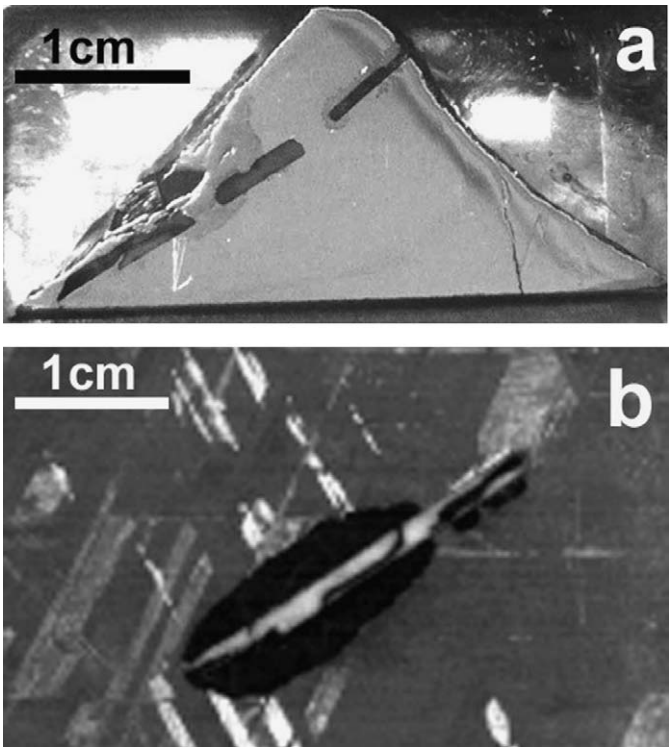

Fig. 6. Tabular tridymite in Gibeon. (a) An apparently discontinuous lamella (dark gray) in UCLA specimen IN590. Reflected light. (b) A similarly-sized, continuous lamella (white) in Vienna Museum of Natural History Gibeon specimen A3; also visible is a dark melted zone and an adjacent undisturbed Widmanstätten structure.

that the tridymite "crystals are oriented perpendicular to the long axes of the inclusion, suggesting that they formed in situ along a preexisting metal surface." We interpret the tridymite platelets to represent veins that were thinner when formed. When contraction of the metal caused the veins to widen, the tridymite minimized its surface energy by forming the observed platelets.

Fig. 6b shows a similarly-sized tridymite plate (0.5–1.5 × 22 mm) in Gibeon specimen A3 from the Vienna Natural History Museum (G. Kurat, pers. comm.). Scott et al. (1996) examined tridymite in Bishop Canyon; an image is shown in their Fig. 6. The tridymite forms two plates about 1 mm thick and 5 and 10 mm in maximum dimension. Ulff-Møller et al. (1995) reported rare cases of centimeter-size tridymite in Gibeon as well.

We did not obtain compositional data for the lamellar tridymites. Ulff-Møller et al. (1995) noted that they have a much lower content of Al and Ti than do the SiO_2 occurrences in SJN and Steinbach, a fact consistent with their formation by condensation in a vein since both Al and Ti are refractory.

4. Formation of the IVA irons from L-LL materials: Overview of the challenges

In discussing possible models for IVA irons we will assume that, as implied by the O-isotopic composition, the primitive IVA asteroid was composed of L or LL chondrite materials. We recognize that the IVA O-isotopic composition could be produced by an admixture of materials that does not include L or LL chondrites, but among the meteorites in our collections there is only one (uncommon) chondrite group (the ordinary-chondrite-related R chondrites) having $\Delta^{17}O$ values more positive than those of LL chondrites, and we therefore find it more reasonable to examine processes by which IVA metal and silicates could form from L-LL chondrite materials. We return to this topic in Section 12.

Although we suspect that low type-3 chondrites such as LL3.0 Semarkona better represent the nature of IVA precursor materials prior to heating and metamorphism, it is useful for discussion to mention that metamorphic equilibration of such materials under closed-system conditions might have produced an olivine composition near Fa28 and a pyroxene composition near Fs25; the latter is about 2× higher than that observed in SJN or Steinbach.

There are two major chemical challenges associated with forming the IVA meteorites from L-LL parental materials. The first is large in scale: the reduction of the Ni content of the metal from L-LL values to the much lower IVA value. The second may be either local or large-scale: formation of SiO_2 and Fs13 low-Ca pyroxene (rather than the olivine expected to crystallize from an L-LL magma) at the IVA core-mantle interface.

As discussed in the Introduction, the mean Ni content of L-LL metal is about 170 mg/g Ni. To convert such metal into initial IVA metal having 83 mg/g Ni, it is necessary to dilute it with a comparable amount of Ni-free Fe.

The mean FeO/(FeO + MgO) ratio in completely melted L-LL silicates would be about 0.27. Complete melting of the silicates would yield a low-SiO_2 (~50 wt.%) liquid that would crystallize olivine as the first liquidus phase. Assuming a $(Fe/Mg)_{solid}/(Fe/Mg)_{melt}$ distribution ratio of 0.3 as recommended by Warren (1986), we calculate that the first crystallizing olivine would have a composition of Fa10; crystallization of pyroxene would give a similar or slightly lower Fe/(Fe + Mg) ratio, i.e., Fs09. In contrast, the IVA silicates are silica-rich and the Fs content of the low-Ca pyroxene is Fs13. We assume that the IVA silicates are representative of those everywhere in the lower mantle of the IVA asteroid, but it is possible that these were uncommon materials formed in special (possibly core-related) processes.

Because the temperature of the IVA metallic magma (estimated below) is high, i.e., ~1800 K at the start of crystallization, the magma cannot be stored on top of silicates, particularly chondritic silicates. This high-temperature magma would have had a viscosity similar to that of water. Thus, at whatever depth the melting of the metal occurs, it would have buoyantly moved to the center of the asteroid on a relatively short time scale. A detailed estimate depends on the volume of magma and the nature of the conduits, and is beyond the needs of this study. We note that the acceleration of gravity at 1 km from the center of the body

Table 3
Sequence of steps in our model to explain the formation of the IVA irons and their silica and silicate inclusions

I	A high-velocity ($\geqslant 7$ km s^{-1}) impact onto a highly porous L-LL-chondrite-like asteroid produced high temperatures at the bottom of a cylindrical impact crater (the part of the asteroid distant from the impact site was relatively unaffected by this event)
IIA	Extensive volatile loss occurred including FeS dissociation and loss of S to space Some FeO reduction occurred with loss of the O to space, in part as CO
IIB	A metallic magma with a volume of a few km^3 was produced; it rapidly (on a scale of about one day) migrated through the porous underlying materials to form a central core
III	After extensive crystallization of the core a second event injected silicates into fissures in the core
IV	The core crystallized through the $\alpha + \gamma$ field while insulated by overlying materials
V	After cooling to about 600 K and forming the Widmanstätten pattern another impact occurred that converted some of the low-Ca orthopyroxene into clinopyroxene

is $\sim$1 cm s^{-2}. If we assume a steady-state velocity of 1 cm s^{-1}, it would require 10^5 s ($\sim$1 day) to move a distance of 1 km. If the melt started 10× farther from the center, the gravitational acceleration would have been 10× higher. Thus, the estimate of $\sim$1 day to reach the center of a highly porous (or fractured) asteroid seems reasonable.

Because our IVA model is unconventional we outline the key steps in Table 3 to help the reader follow the interpretations that follow.

5. Temperatures in the IVA core and associated materials: Possible heat sources

5.1. Initial temperature of the IVA metallic magma and the precursor materials

The mean initial temperature of the initial IVA magma provides a lower limit on the mean temperature of the chondritic precursor materials from which the magma separated. The magma temperature is mainly determined by the S content; this was estimated to be 25 mg/g by Scott et al. (1996) but only 4 mg/g by Wasson and Richardson (2001). Our best current estimate, and the one used in the crystallization modeling discussed below, is 5 mg/g.

We estimated the relevant temperatures by first reading them off the Fe–S phase diagram (Brandes and Brook, 1992) and then lowering them by 20 K to allow for the effect of the initial Ni content (estimated by Wasson and Richardson, 2001) of 83 mg/g. The Fe–S phase diagram yields a liquidus temperature of $\sim$1793 K for 4 mg/g S and 1749 K for 25 mg/g S, lowered to 1773 and 1729 K, respectively, to allow for the effect of Ni. We will use a value of $\sim$1770 K, corresponding to our current S estimate of 5 mg/g. This is a lower limit on the actual mean temperature; if all metal melted, a modest increase in the actual temperature would not have affected the S and Ni contents used to obtain the estimate. This mean temperature applies to the system that includes the metallic melt and the associated silicate melt and solids, a region that (based on L-LL chondrite compositions) was probably about 5–6× more massive than the IVA core. Note that 1770 K is 510 K higher than the Fe–FeS eutectic temperature of 1260 K, and is high enough to produce extensive melting of the silicates if some low-melting phases such as plagioclase were present. Also, the enstatite–tridymite eutectic temperature is $\sim$1770 K. A successful heat source must thus account both for an increase in temperature and for a considerable quantity of latent heat.

5.2. Internal heating of the IVA asteroid by short-lived radionuclides

Discussions in the recent literature are focused on two main asteroidal heat sources: the decay of the extinct radionuclide ^{26}Al (and possibly also ^{60}Fe) and the deposition of heat by massive impacts. The adequacy of both has been challenged. Recent data on chondrules indicate ^{26}Al/^{27}Al ratios were too low to produce differentiation (e.g., Kunihiro et al., 2004), and some past evaluations of impact processes have concluded that these produce little heating in the Asteroid Belt >2.2 AU from the Sun (e.g., Keil et al., 1997).

The initial ^{26}Al/^{27}Al ratios preserved in the unequilibrated chondrites range from high values in refractory inclusions to low values in chondrules. Assuming that the Al isotopes were well mixed, at least within the nebular formation regions of the individual chondrite groups, it is the lowest preserved ratio that must be used in asteroidal heating calculations. Thus, the relatively high inferred initial ^{26}Al/^{27}Al ratios for some chondrules from CV3 Allende reported by Bizzarro et al. (2004) are not relevant to the discussion of asteroidal heating.

The initial ^{26}Al/^{27}Al ratios in LL3.0 Semarkona chondrules, shown by Kita et al. (2000) to be about 7.5×10^{-6}, provide an excellent data set for evaluating the potential of an ^{26}Al heat source in an L-LL asteroid. Kunihiro et al. (2004) showed that the mean ratio is too low to melt and differentiate an asteroid even if it formed immediately after chondrule formation and even if the asteroid were large enough to retain all interior heat. These workers calculated that the ^{26}Al content could raise the temperature of the L-LL body to 1360 K (neglecting latent heat). There is enough heat to melt the FeS and some metal, but no silicates would melt. The evolved heat is only about half of that (including latent heat) required to produce the temperature of ca. 1800 K inferred for the IVA core.

As discussed by Kunihiro et al. (2004), it is possible that differentiated asteroids formed as a result of radiogenic heating from chondritic materials having ^{26}Al/^{27}Al ratios $\geqslant$2× higher than those in LL chondrules. However, as of

now there are no studies that document the existence of initial ratios in planetesimals higher than those measured in LL3.0 Semarkona chondrules by Kita et al. (2000). The required high ratios therefore remain speculative.

There are conflicting reports about the initial $^{60}Fe/^{56}Fe$ ratios. Tachibana and Huss (2003) reported an initial $^{60}Fe/^{56}Fe$ ratio in LL3.1 Bishunpur and Krymka of 1.4×10^{-7} that, according to Kunihiro et al. (2004), would increase temperatures by only 160 ± 20 K. In contrast, a recent study by Mostefaoui et al. (2005) reported a ratio 7× higher, 9.2×10^{-7}. LL-chondritic matter with Fe having the latter ratio and Al with the Kita et al. $^{26}Al/^{27}Al$ ratio could produce moderate degrees of melting, although, after allowance for latent heat, would only marginally reach the 1770 K temperature inferred for the IVA core.

Until the $^{60}Fe/^{56}Fe$ ratio has been better defined we find it best to assume that radiogenic heating alone was inadequate to melt the IVA asteroid and suggest that the asteroid was largely melted by a massive impact. We suggest that the impact occurred when the parent asteroid was still highly (>50%) porous; the higher the porosity, the more efficient the conversion of impact kinetic energy into heat (Melosh, 1989).

A complicating isotopic discovery is the ^{182}Hf–^{182}W study by Kleine et al. (2005) which showed that $^{182}W/^{184}W$ ratios in samples of magmatic iron meteorites (including IVA) are lower than the initial ratio obtained by interpreting data on separates from a refractory inclusion from the CV3 Allende as an isochron. This implies that the irons formed earlier than refractory inclusions. Because Allende has experienced extensive aqueous alteration, it seems possible that the low-Hf (magnetic) sample has been contaminated by radiogenic ^{182}W. We suggest that this result needs to be confirmed on a more pristine meteorite before it is used as a chronological constraint on iron-meteorite formation.

For completeness we also mention that another type of internal heating has been proposed. Joule heating by currents induced by a T-Tauri solar wind (e.g., Sonett et al., 1970) might also be able to provide an internal heat source. However, the model is largely undeveloped; many problems need to be solved (e.g., the role of porosity and random orientation of spin axes) before this can be considered a viable mechanism.

5.3. Impact heating of the IVA precursor materials on the parent asteroid

The chief arguments against the impact production of asteroidal magmas is that the mean impact velocity of 5 km s^{-1} in the Asteroid Belt provides relatively little energy per unit projectile mass, and that, because of the low escape velocities (ca. 0.14 km s^{-1} for an asteroid with a radius of 100 km and chondritic density), the most strongly heated crater ejecta is lost from the asteroid (Keil et al., 1997). There are several problems with this paper. The discussion of cratering is based on terrestrial analogs that are highly compact, and thus produce bowl-shaped craters with appreciable amounts of high-temperature ejecta leaving the crater at velocities greater than the escape velocity of the asteroid. The second main problem is that the authors assume that the whole asteroid must be heated.

However, as discussed in some detail by Wasson and Kallemeyn (2002), modeling by W. Bottke (pers. comm., 2001) has shown that 20% of impact velocities are 7 km s^{-1} or higher, and it is clear that minor impacts on highly porous bodies result in retention of most of the heat. Our picture of the IVA impact event and similar magma-generating impacts is that, because of the high-porosity of the target asteroid, the heat was mainly deposited at the bottom of quasi-cylindrical craters having depth/diameter ratios > 1.

H.J. Melosh (pers. commun., 2005) carried out a planar-impact approximation and showed that the minimum velocity required to produce appreciable melting in a highly porous target is 4 km s^{-1}. It would appear that an impact velocity of 7 km s^{-1} is marginal for producing the high (1800 K) temperatures experienced by the IVA parental materials, and that this should be considered a lower limit on possible impact velocities.

Only large-scale impact events are likely to produce magmas large enough to fractionally crystallize. Nonetheless, it is not necessary that asteroid-size amounts of melt be produced. The flux of IVA iron meteorites onto the Earth requires about 1 km^3 of IVA materials in heliocentric orbits; thus, the total amount of chondritic material that was melted could be as small as 5 km^3. Note that the size of the asteroid is not specified in this model. We suggest that the radius was probably small, perhaps 10–20 km. Small radii make it more likely that the molten metal can drain to the center of the body with only minimal loss by freezing as a result of heat exchange with the cooler intervening materials.

In impact events the heat is distributed heterogeneously, as demonstrated in meteorites such as Portales Valley in which massive metal veins and some essentially unmelted H-chondrite materials occur on a scale of ~10 cm (Rubin et al., 2001). We suggest that, immediately after a large impact, such thermal heterogeneities were present at scales of 10 cm to several kilometers in the portion of the IVA asteroid affected by heat from the impact event. The combination of heat and rarefaction waves caused moderate expansion of the hottest materials, but because of the geometry they were largely confined to the cylindrical crater.

We considered two possible kinds of impactors that are consistent with the O-isotopic data. One is another local L- or LL-like body which happened to have had an orbit that led to an impact with a relatively high (7 km s^{-1}) velocity. The projectile might contribute an appreciable fraction (e.g., >20%) to the resulting magma but, because its O-isotopic composition was similar to that of the target materials, the melt had an L-LL composition. In the second model we envision the higher velocity impact of an object

from the outer solar system. The mean velocities of Oort cloud comets are about 40 km s^{-1} at 2.5 AU, those of bodies from the Neptune region were smaller but >10 km s^{-1}. Outer-solar-system bodies might have an O-isotopic composition similar to those in carbonaceous chondrites, with $\Delta^{17}O$ in the range from −3 to +1‰. However, because the projectile would have contributed <5% of the mass of the silicate magma, it would have produced a relatively minor change in the $\Delta^{17}O$ value of the magma.

What actually happens in the hot impact debris depends on the kinetics of the dissociation and evaporation reactions, and these in turn will depend on the physical state of the hot materials. We have not tried to model these processes and states, but have instead carried out a few equilibrium calculations based on rough ideas of the physical processes involved.

5.4. Impact heating, radionuclide or other internal heating, and volatile loss

Impact heating is an extremely rapid and highly heterogeneous heating process; internal (radionuclide or joule) heating is a very slow and uniform heating process. Impact heating occurs in surficial layers of a chondritic asteroid; radionuclide heating is most effective in the interior of the asteroid. It is important to recognize that, because of these differences, the heating of asteroidal materials from low (ca. 200 K) to high (ca. 1800 K) mean temperatures should produce very different products.

For example, we estimated above that the initial temperature of the IVA metallic magma was 1770 K, and it might have been higher. Kunihiro et al. (2004) estimated that plagioclase melts in the range 1400–1500 K; thus, it seems probable that, when an asteroid heated by ^{26}Al reaches a temperature of 1500 K, a melt with basaltic composition would form and, as a result of buoyancy forces, would migrate towards the surface, taking with it the ^{26}Al. This process, which would occur after about 1–3 ^{26}Al half-lives, would bring much of the ^{26}Al to the surficial parts of the asteroid where the heat is more efficiently transported to the surface and radiated into space (e.g., Taylor et al., 1993). As a result, the interior of the asteroid would no longer be heated, and it would not be possible to reach the IVA magmatic temperature of 1770 K.

In addition, the rapid time scale of impact heating seems better suited to the loss of volatiles than is slow internal heating. As noted by Wasson and Trigo-Rodriguez (2004), volatilization produced during chondrule formation must have resulted in the recondensation of the evaporated elements as fine (<1 μm) condensates, mainly formed on the surfaces of fine nebular particles. During impact-generated flash heating of a highly porous chondritic material, it seems likely that large fractions both of these very fine deposits and their fine substrates would be evaporated. Depending on the details of the circumstances (e.g., whether a hot carrier gas, perhaps H_2O, is also generated), efficient loss of volatiles may have occurred.

The important message is that, in asteroidal size bodies, impact heating is better suited than internal heating both for the loss of volatiles and for the generation of high-temperature magmas.

6. Large- and small-scale reduction processes in the IVA asteroid

6.1. Processes that can produce reduction and reducing agents

There are two reduction processes that must have occurred if IVA materials formed from L-LL precursors: the formation of the Fe metal necessary to reduce the bulk Ni content of the IVA magma from ca. 170 to 83 mg/g, and the formation of the SiO gas that seems necessary to explain the formation of SiO_2 veins. The formation of low-Ca pyroxene rather than olivine at the core-mantle interface may also be related to the reduction process that led to the Ni dilution in the metal. The Ni dilution process was certainly large-scale; it may have involved five or more cubic kilometers of largely molten matter and final temperatures of ~1800 K or higher. The process responsible for the formation of tabular SiO_2 in Gibeon and Bishop Canyon may be large or small in scale.

It is possible to reduce FeO and FeS to metallic Fe with temperature alone in an open system. The FeS bond breaks at relatively low temperatures (<2000 K) and the FeO bond is weaker than those involving oxygen and the other common metals Mg and Si. If, as seems likely, there was loss of a gas phase during the hypothetical impact event, then there is little doubt that minor-to-moderate reduction of FeS and FeO occurred.

Ulff-Møller et al. (1995) reviewed several possible reducing agents that might have affected the IVA meteoritic materials. The chief reducing agent in ordinary chondrites is probably C in one of its forms. Jarosewich (1990) reported total C contents in LL3.0 Semarkona and LL3.1 Bishunpur of 5.7 and 5.3 mg/g, respectively. As will be shown below, this amount of C is enough to produce about half the required FeO reduction; if the projectile originated in the outer solar system, it may have had an appreciably higher C content. Most chondritic C is in the form of carbonaceous matter associated with the silicates, but there may also have been carbides or graphite associated with the metal.

6.2. Reduction of silicates and FeS to produce the observed IVA Ni concentration

As stated above, formation of the IVA core from L-LL metal having 170 mg/g Ni requires that the original metal be diluted with a roughly equal amount of Ni-free Fe metal. The obvious way to create such low-Ni metal is the reduction of FeS and of FeO in the silicates. The amount of NiS in the FeS and of NiO in LL3 silicates is very low (typically <0.5 and <0.04 wt.%, respectively; e.g., Jones,

Table 4
Fractions of Fe in different phases of the hypothetical L-LL chondrite parent (a mix of 2 parts L and 1 part LL compositions) of the IVA metal

Form	Mass (g/1000 g)	Mass of Fe (g/1000 g)
FeO	153	119
FeS	59	37
Metal[a]	68	56
Reduced Fe[b]	—	71

[a] Metal compositions based on Fe metal in unweathered observed falls from Jarosewich (1990) and Ni and Co values from Wasson and Kallemeyn (1988).
[b] Fe needed to lower Ni content of the metal from 170 to 83 mg/g.

1990), although some LL3 chondrites contain accessory pentlandite [$(Fe,Ni)_9S_8$] formed during parent-body aqueous alteration. In general, however, the reduction of sulfide and FeO in silicates would produce nearly pure Fe metal.

Table 4 provides a perspective for the inferred reduction process. We assume that the precursor of the IVA materials consisted of a mixture of 2/3 L and 1/3 LL materials, and calculated the compositions of the Fe-bearing components of these using the FeO, FeS, and Fe metal data of unweathered falls from Jarosewich (1990). The Ni and Co contents of unweathered falls were taken from Wasson and Kallemeyn (1988). In the central column are the concentrations in grams per 1000 g of FeO, FeS and metal in our hypothetical precursor, and in the right column we show the amount of Fe in these components. The last line in the third column shows that 71 g of Fe per 1000 g of starting L-LL material must be reduced from FeS and/or FeO in order to lower the Ni content of the metal from 170 to 83 mg/g.

We noted above that impact heat is distributed heterogeneously, and that the mean temperature of the core and associated silicates was >1770 K. However, we have no direct information about the maximum temperatures that were reached or about the scale of the heterogeneities.

We know of no published discussion of the manner in which heating occurs in the central part of a moderate-size impact event during the period immediately following the initial compression state. To facilitate the discussion of heat redistribution during this stage, we suggest the following, very crude, three-component scenario: (a) slightly heated, coarse, solid materials, perhaps ~500 K; (b) largely melted materials, perhaps ~1500 K; and (c) vaporized (and ionized) materials, a plasma perhaps at ~5000 K. The fraction of the target and projectile in each component will vary widely depending on the impact velocity and the physical properties of both the target and the projectile.

The most porous materials will be heated the most during the compression phase; these probably included all kinds of chondritic materials (chondrules, metal, fines, etc.). Post-shock, the heat will be redistributed among the three components. In particular, those materials in contact with the plasma will gain heat. Because heat conduction is a slow process, the materials that gain the most heat will consist of thin surficial layers.

As discussed by Wasson (1996) and Wasson and Trigo-Rodriguez (2004), chondrule formation inevitably led to large amounts of evaporation of the fine nebular materials. These materials immediately recondensed as fine smoke or onto the surfaces of preexisting grains. The interchondrule matrix may have largely formed in this way and the most volatile elements (including S as FeS) will probably be largely sited in these surficial deposits. Even though some of the evaporated Fe may have been metallic, recondensation at low (<500 K) temperatures will result in the formation of Fe–O (and Fe–S) bonds. Grossman and Brearley (2005) have demonstrated that much of the bulk S in chondrites occurs in fine grains. In addition to the materials that were formed as fine grains in the nebula there will be another population of fine, dispersed, solid and melt particles produced by the compressional phase of the impact; these were also efficiently heated by the plasma.

Thus, impact events are well suited to the loss of volatiles by the IVA precursor materials, either as a result of evaporation of entire tiny particles or as a result of the loss of volatile species from molten materials.

Hot melt droplets are expected to lose much of their S. We examined several possible reactions. Perhaps the most relevant reaction in the melt is

$$2FeS(l) = 2Fe(l) + S_2(g) \quad (1)$$

Using Gibbs free-energy data from JANAF (1998) and assuming unit activities for FeS and Fe, we find that this reaction yields an S_2 vapor pressure of 10^{-3} atm at ~1900 K.

It would be difficult to model the actual conditions of a diverse mix of components having a wide range of temperatures in this expanding, turbulent impact plume. We suggest that, as a crude approximation, one can use equilibrium calculations carried out for the solar nebula to assess which elements are the most likely to be lost. To the degree that loss mainly resulted from the volatilization of late nebular condensates onto grain surfaces, this approximation is quite suitable. The redox conditions may have differed from those in the nebula. It seems probable that the H_2/H_2O ratio was orders of magnitude lower than that in the nebula (implying more oxidizing conditions) but vaporization of carbonaceous matter present in the hypothesized late nebular condensates would have made conditions more reducing.

Large amounts of S loss are indicated by the inferred compositions of the IVA cores. The data of Jarosewich (1990) yields a S/Ni weight ratio of 1.9 for our L-LL precursor mix. The estimated S content of the IVA metal magma of Scott et al. (1996) of 25 mg/g yields a S/Ni ratio of 0.30; our estimate of 5 mg/g gives a ratio of 0.060. Thus, the magma is inferred to have lost 84% to 97% of its S during formation; we conclude that loss of S from FeS provided about half (~35 g) of the required 71 g of Fe (Table 4). The remainder must have been produced by reducing FeO from the silicates.

The FeO may have been reduced by an agent such as C or, at high temperatures, by disruption of the FeO bond followed by loss of O from an open system. We will first discuss reduction by C. One obtains essentially the same result whether one reduces solid FeO, $FeSiO_3$ or Fe_2SiO_4 (the free energy of formation of the latter two from the oxides is relatively small, i.e., several kJ). We will use Fe_2SiO_4 in our example:

$$Fe_2SiO_4(s) + C(s) = FeSiO_3(s) + Fe(s) + CO(g) \quad (2)$$

If we assume unit activities for all solid phases, the free-energy data (Robie et al., 1978; Berman, 1988; JANAF, 1998) indicate an equilibrium constant (=pCO) of 228 atm at 1500 K and 680 atm at 1700 K. It seems clear that the pCO would be similar or larger in the molten system (at somewhat higher temperatures). These pressures imply near-complete loss of CO gas to space following the impact.

If CO is lost, reaction (2) goes to completion. We mentioned above that the most primitive L and LL chondrites have C contents of about 5.6 mg/g; because one mole of Fe is produced by every mole of C oxidized to CO, 5.6 g of C can reduce 26 mg of Fe, about 37% of the Fe needed to reduce the Ni content of the metal from 170 to 83 mg/g.

The reducing capacity of graphite is twice as large if CO_2 is the product rather than CO. However, equilibrium calculations at temperatures of 1500–2000 K indicate that the pCO/pCO_2 ratio is about 35–40 in systems in which the activity of FeO (or $FeSi_{0.5}O_2$) is ~0.15; thus, the amount of additional Fe metal associated with CO_2 formation is negligible. And, during the short time available for reaction in an impact-heated assemblage, formation of diatomic CO would occur much more efficiently than formation of triatomic CO_2.

The third mechanism to obtain reduced Fe is to break the FeO bond at high temperatures:

$$FeO = Fe + O(g) \quad (3)$$

and

$$FeO = Fe + \frac{1}{2}O_2(g) \quad (4)$$

The physical form of the FeO was taken to be the stable form at a pressure of 1 atm; solids below 1800 K (FeO) or 1900 K (Fe), liquids above these temperatures. Our calculations show that appreciable pressures of O(g) and O_2(g) are only reached at temperatures >2500 K. At 2500 K, pO is about 10^{-5} atm and pO_2 about 4×10^{-7} atm. If the gases escape, the reactions proceed to the right as written, but at such low vapor pressures the reaction rate is relatively low. Nonetheless, in those portions of the impact melt that reached temperatures >2500 K, there could have been appreciable open-system loss of O or O_2. Wang et al. (2001) evaporated chondrite material under vacuum conditions and observed that, at 2270 K, a 200 mg sample lost >90% of its FeO within about 4 min. Because of the oxidizing conditions the remaining Fe formed Fe_3O_4 instead of metal. We suggest that, under reducing conditions, evaporation of FeO followed by dissociation should be able to provide much of the additional 6–10 g of Fe required to account for the low IVA Ni content. We suggest that the expanding vapor cooled enough to condense Fe(g) to Fe (s) which entered the metallic melt whereas the O and its gaseous reaction products largely escaped from the asteroid. The retention of the Fe is consistent with the fact that several moderately volatile elements such as As and Au were not lost from the IVA system.

Group IVA did lose two more-volatile moderately volatile elements, Ga and Ge. The mean L and LL compositions given by Wasson and Kallemeyn (1988) yield mean Ga/Ni and Ge/Ni mass ratios of 4.8×10^{-4} and 8.6×10^{-4}, respectively; the mean IVA compositions given by Wasson and Richardson (2001) are 3.6×10^{-5} and 1.9×10^{-6}, respectively, 1–2 orders of magnitude lower than the L-LL ratios. These imply 93% loss of Ga and >99% loss of Ge during formation.

To summarize, we calculate that, in a hypothetical 1000 g of L-LL parental material containing 68 g of metal with a Ni concentration of 170 mg/g, it was necessary to add 71 g of Fe to reduce the Ni content down to the observed 83 mg/g in the IVA core. We suggest that about half of the required Fe was the product of FeS dissociation and loss of S_2 from an open system. The other half of the Fe must have been reduced from the silicates; we infer that most of this reduction was by C contained in the precursor materials or the projectile, with the remainder resulting from thermal dissociation of FeO. This reduction involved about 30% of the FeO in the mafic silicates. During the heating events the IVA materials lost >90% of their Ga and Ge.

6.3. Reduction as an explanation of IVA silicate compositions

The same reduction process required to bring the Ni content of the metal from the L-LL range down to that inferred for the group-IVA magma would also have reduced the FeO/(FeO + MgO) ratio in the associated mafic silicates from ~0.27 down to 0.206 (note that reducing FeO by 30% only reduced this ratio by 24%).

If the reduced L-LL mix melted completely, calculations (Roeder and Emslie, 1970; Warren, 1986) show that the first olivine or pyroxene that would crystallize under equilibrium conditions would be expected to have FeO/(FeO + MgO) ratios of about 0.074, appreciably lower than the ratios (about 0.13) observed in SJN and Steinbach pyroxene.

We suggest four possible explanations for this discrepancy: (1) the difference could either reflect non-equilibrium crystallization of the initial melt or that the pyroxene was not the first mafic mineral to crystallize from the melt; (2) the mafic cumulates at the core-mantle interface may have included residues that were not reduced during the hypothesized melting event; (3) the SJN and Steinbach materials

may have formed by partial melting of the mantle mafics; or (4) the first cumulate may have been magnesium olivine, but a later evolved liquid (such as that proposed by Ulff-Møller et al., 1995) could have produced more ferroan pyroxene in SJN and Steinbach.

In contrast, the tridymite cannot be easily explained by these simple models. We find subsolidus reduction to be more promising formation mechanism, and now pursue this process in greater detail in Section 7.

7. Formation of tridymite veins in Gibeon: Role of reducing gases

We suggest that the fact that the morphology of tridymite in Gibeon and Bishop Canyon indicates that it was deposited in veins is an important clue to understanding the origin of the tridymite in the other IVA irons. Because these were deposited in fissures in the solid metal of Gibeon and Bishop Canyon, they formed after the large (30%) estimated degree of crystallization.

The mean SiO_2 abundance is not known. If it were as high as 1 mg/g it should be visible in most Gibeon surfaces having areas of 100 cm^2. It is clearly much rarer; we suggest that the mean concentration is in the range of 0.1–1 μg/g.

It is probable that the lamellar tridymite in IVA irons formed by deposition from a supersaturated fluid. We infer that the components of SiO_2 were transported by dry, gaseous fluids. It is important to examine processes that could have produced the volatile Si-rich phase. SiO_2 itself has a very low vapor pressure, and it is not plausible to suggest that SiO_2 (g) was the main Si species in the gas. In contrast, SiO is quite volatile; thus, reducing conditions would have made it much easier to transport the Si into (or within) the interior of the IVA core at high temperatures and, following a drop in temperature, to precipitate tridymite.

Reduction of SiO_2 or $FeSiO_3$ from the mantle could have produced the SiO(g). One possible reducing agent is CO, with the resulting oxidized form being CO_2. Reactions involving CO could be:

$$SiO_2(s) + CO(g) = SiO(g) + CO_2(g) \quad (5)$$

and

$$FeSiO_3(s) + 2CO(g) = Fe(s) + 2CO_2(g) + SiO(g) \quad (6)$$

Less probable is that there was sufficient H_2 to serve as the reducing agent. We used equilibrium calculations to investigate these possibilities; the two reactions give similar results. We assessed the pSiO values at a series of assumed equilibrium pCO/pCO_2 and pH_2/pH_2O ratios; the results are shown in Fig. 7.

If some fraction of the gaseous products of these equations moved into veins and other cavities in the solid IVA core, cooling would cause the reaction to proceed in the reverse direction and produce SiO_2 during cooling. However, the pSiO pressures shown in Fig. 7 are too low to produce appreciable deposits of SiO_2. We therefore conclude that a stronger reducing agent is required.

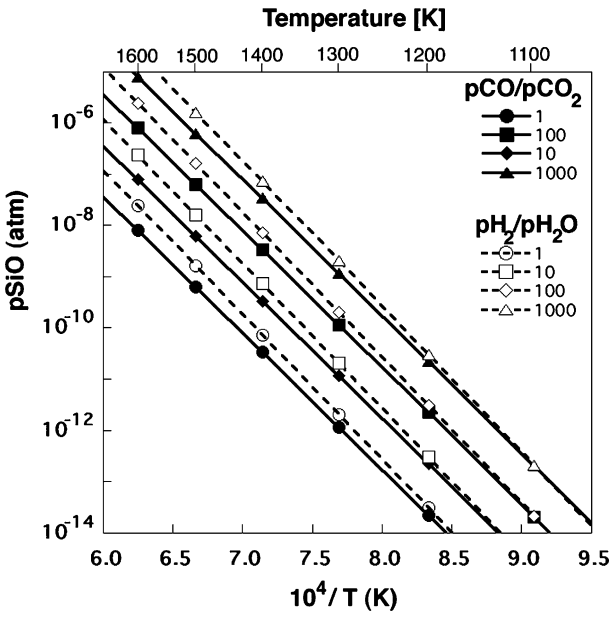

Fig. 7. Gibbs' free-energy-based calculations of equilibrium relationships for reactions involving either CO or H_2 to produce pyroxene and eventually silica from fayalite in the IVA asteroid. Equilibrium pressures of SIO seem too low to account for the formation of the observed tridymite lamellae.

Perhaps the reducing agent was a very small amount of C dissolved in the IVA magma; Moore et al., 1969b reported C concentrations of ~100 μg/g in IVA irons, and initial concentrations were presumably higher. If we assume an initial C content of 400 μg/g, an activity coefficient at 1700 K of 0.1 for C in metallic Fe–Ni, and that $p\mathrm{SiO} = p\mathrm{CO}$, we obtain equilibrium pressures of 1.4×10^{-4} atm for the latter, sufficient to condense tridymite at mean concentrations of 0.1 μg/g in regions having 1% porosity.

Alternatively, as Ulff-Møller et al. (1995) suggested, there may have been a tiny (perhaps 0.1–0.01 mg/g) amount of Si dissolved in the melt. In this case, oxidation, perhaps by O dissolved in the metallic magma or by CO, CO_2 or H_2O vapor from the mantle, would be required to produce the SiO vapors. An intriguing possibility is the reaction

$$Si(l, Fe–Ni) + CO_2(g) = SiO(g) + CO(g) \quad (7)$$

If this reaction is added to reaction (5) we obtain the reaction for Si as a reducing agent:

$$SiO_2(s) + Si\ (l, Fe–Ni) = 2SiO(g) \quad (8)$$

The presence of metallic Si in the core would require it to have been more reducing than the overlying mantle. If, as hypothesized above, the core was formed by an impact event, it seems plausible that heterogeneities in the reduction process would have resulted in the introduction of small amounts of C or Si into the metallic magma.

In summary, it seems plausible that SiO_2 concentrations in the range 0.1–1 μg/g could have been introduced into the core and that the tridymite abundance in Gibeon is not inconsistent with this estimate.

8. Impact melting: Formation of a central core

We noted in Section 4 that, because of the high temperature of the metallic magma, it is inevitable that it will migrate to the gravitational center of the parent asteroid. Its temperature was ~1770 K when it started to crystallize; if, as we suggest, it was formed by melting and minor vaporization during an impact event into a highly porous target, its formation region may have been separated from the center of the body by several km to several tens of km (we assume that the radius of the parent asteroid was relatively small, perhaps 10–20 km).

Shortly after the impact, molten metal and molten silicates would have been in the bottom of the crater (because they formed there or migrated there). In our hypothesized porous asteroid these would immediately have started to flow through cracks to lower levels. The leading edge may have sometimes experienced pooling because the conduit narrowed, but flow-induced erosion would have soon widened these early channels.

If some crystallization of the metal occurred as a result of heat exchange with silicates through which the metal was passing, this would have left some refractory (high Ir, low Au) metal behind. This may be the explanation of the observation that the initial Ir/Au ratio in the IVA magma was only about 64% of that in LL metal (Wasson and Richardson, 2001).

The melt would have been mainly metallic but, if the flow was turbulent, small silicate droplets could have been entrained and carried all the way into the central core. These molten materials may have included some of the most strongly heated silicates, i.e., they may have been partially reduced and have had low contents of volatiles (e.g., Na, Ga) that are lost with the gas phase in impact-generated reducing environments. When core formation was complete, these silicates would have buoyantly separated from the metal.

An interesting question is the detailed heat transfer following emplacement of a hot metallic magma below a substantially cooler layer of silicates. Although it is possible that the adjacent silicates were considerably (200–800 K) cooler than the metallic magma, heat would be rapidly transferred by the melting of plagioclase and calcic pyroxene and the upwards migration of a basaltic melt into the porous body. In this way temperatures of ca. 1500 K would be achieved rather quickly in a thin surrounding shell.

A large amount of heat became available when the magma crystallized. Wasson (1996) noted that the heat released by the crystallization of 1 g of Fe metal (247 J/g) is about 200× greater than the heat (~1.2 J/g) required to increase the temperature of silicates by one degree.

This scenario suggests that the core initially cooled rapidly but that the rates had dropped an order of magnitude when the last IVA iron crystallized at a temperature around 1700 K. Modeling this high-temperature cooling is beyond the scope of this paper. It should cause no resolvable effect on the low temperature (600–700 K) cooling rates that are recorded in the Widmanstätten pattern. If high cooling rates resulted in incomplete mixing of the metallic magma it could have had an effect on the trends on element-Au diagrams; perhaps the increase in the negative slope on IVA Ir–Au and Ir–As diagrams (Fig. 8) at Au = 0.9 μg/g is partly due to this effect.

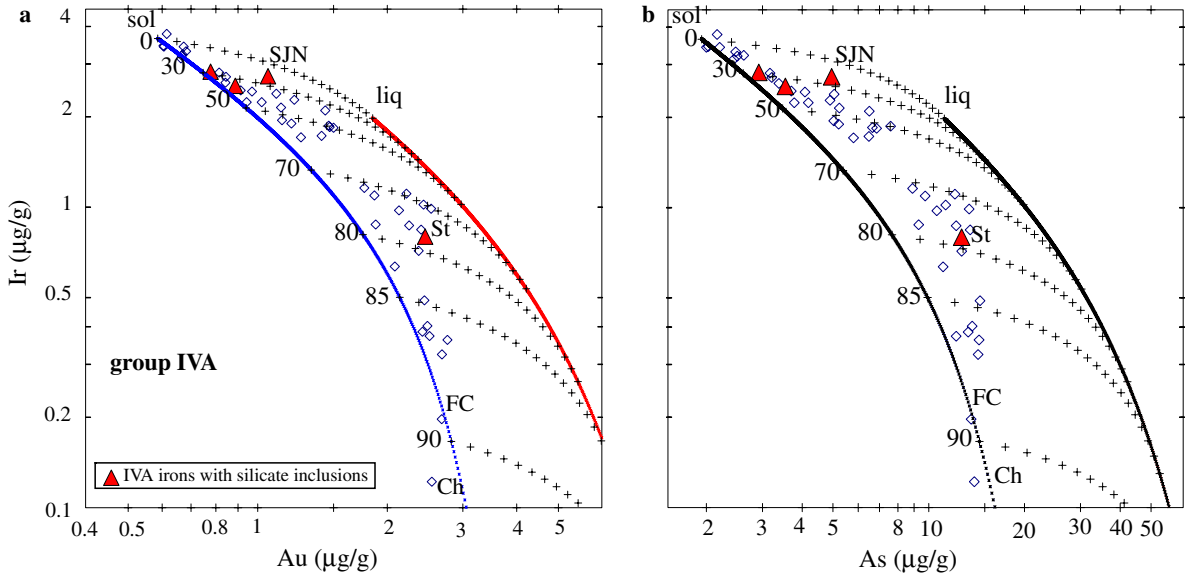

Fig. 8. Calculated tracks of liquid and solid compositions of IVA irons based on a fractional crystallization model. (a) log Ir vs. log Au. (b) log Ir vs. log As. Mixing curves connect these tracks at seven different degrees of crystallization (e.g., 0%, 30%, and 50%). Approximately half of the IVA irons formed within the first 60% of the core to crystallize, the remainder during the 70–90% crystallization interval. The four silica-bearing IVA irons are represented by shaded triangles.

9. Introduction of silicates into the IVA melt: Relationship to the degree of crystallization of the IVA core

In Table 5 we list mean metal compositions of the four silica-bearing IVA irons. Data for these and other IVA irons are given by Wasson and Richardson (2001). In Fig. 8 these compositions are plotted on Ir–Au and Ir–As log–log diagrams. Group IVA is one of three large iron meteorite groups that show clear evidence of near-ideal fractional crystallization. This process requires complete mixing of the melt on a time scale that is short relative to the period necessary to crystallize a small amount (say 1%) of the remaining liquid. The key parameter controlling this crystallization process is the solid/liquid distribution coefficient $D = X_{sol}/X_{liq}$ (where X_{sol} is the elemental concentration in the solid and X_{liq} is that in the parental melt, i.e., "the mother liquor"). For most refractory elements, $D > 1$; for most volatile elements, $D < 1$. As shown in numerous studies, most recently by Chabot and Jones (2003), D values depend on the composition of the metallic magma, and particularly on the S content of the magma.

As discussed in Wasson (1999) and Wasson and Richardson (2001), the scatter in the elemental concentration data for magmatic irons on diagrams such as those in Fig. 8 far exceeds experimental (analytical and sampling) error. Based especially on the trends within the group-IIIAB Cape York irons, Wasson (1999) showed that the scatter could be the result of melt trapping, which produces arrays connecting the equilibrium solid and liquid compositions. In addition to the mixing of melt and solid that are in equilibrium, there is also evidence for the occasional mixing of early solids with much more evolved melt.

Crystallization causes the fully incompatible elements S and P to increase in the residual melt. As a result most D values increase during crystallization. Some researchers (e.g., Chabot, 2004) argue that the crystallization trends in magmatic iron-meteorite groups should be based on trends fitted to laboratory D values, with the S content the only free parameter. In contrast, Wasson (1999) has argued that, because of the high degree of scatter in the laboratory data, particularly at the low S concentrations that are most relevant, the published fits to the data are relatively inexact and therefore quite permissive. He suggested that the trends within each group are best obtained by trial and error fits of D-value algorithms within the range permitted by uncertainties in experimental data. In a few cases (IIIAB Cape York is the prime example) the S content of the magma can be directly estimated from a combination of observed (modal) S contents and elemental fractionation trends.

Wasson and Richardson (2001) developed a single quadratic fit of the relationship between log D and the log S concentration of the melt for both IVA and IIIAB trends. Here we return to a linear fit of the dependence of log D on the S content to obtain IVA D values. Fig. 8 shows IVA metal compositions, the calculated solid and liquid tracks together with mixing curves connecting these tracks at seven different degrees of crystallization (0%, 30%, etc.). Based on the present modeling attempt, about half of the IVA irons formed within the first 60% of the core to crystallize, the remainder during the period of 70–90% crystallization. We chose D values for Au and As that give both a satisfactory fit to the broad downward trend of the left envelope (i.e., zero trapped melt) of the distribution and also yield similar estimates (on each diagram) of the fraction of trapped melt in each iron. We used the parameterization given by Jones and Malvin (1990):

$$\ln(D) = \beta_{sp} \cdot \ln(1 - 2 \cdot \alpha \cdot X_s) - (4 \cdot \alpha \cdot X_p) + C, \quad (9)$$

where $\beta_{sp} = [2X_s/(2 \cdot X_s + 4 \cdot X_p)] \cdot \beta_s + [4 \cdot X_p/(2 \cdot X_s + 4 \cdot X_p)] \cdot \beta_p$. The values of the constants for the three elements modeled in Fig. 8 are given in Table 6.

We found it particularly challenging to find fits for D_{Au} and D_{As} that would yield similar degrees of melt trapping for each diagram, but finally had a modicum of success. Note, for example, the position of Steinbach on each diagram. On the Ir–Au plot the position corresponds to about 22% trapped melt, on the Ir–As plot, to about 18%. We consider this to be adequate agreement considering the uncertainties in the concentration data and the approximations inherent in the fitting procedures. The SJN composition implies about 21% trapped melt on the Ir–Au and Ir–As diagrams.

The positions of the four silica-bearing IVA irons are shown in Fig. 8 by shaded triangles. As mentioned earlier,

Table 6
Values of the constants used in equation 15 to calculate the dependence of D_{Ir}, D_{Au} and D_{As} on the S and P content of the magma

Element	C	β_s	β_p
Ir	0.48	−4.5	−4.0
Au	−1.15	0.00	0.00
As	−1.77	−0.50	−0.30

Table 5
Elemental composition of the metal in silica-bearing IVA irons

	Cr	Co	Ni	Cu	Ga	Ge	As	W	Re	Ir	Pt	Au
Bishop Canyon	329	3.92	75.8	156	2.06	0.110	2.92	0.60	345	2.83	5.7	0.777
Gibeon	214	3.86	77.4	168	2.09	0.111	3.54	0.61	249	2.54	5.9	0.887
SJN	31	3.89	80.2	162	2.13	0.118	4.95	0.54	322	2.73	5.7	1.057
Steinbach	534	4.22	94.0	164	2.27	0.134	12.7	0.43	120	0.798	4.6	2.500

The first three have relatively high Ir contents, whereas that of Steinbach is relatively low. The data are plotted in Fig. 8.

three of the four have high Ir contents indicating formation early, after about 30% crystallization (SJN about 26%). In contrast, our modeling indicates that Steinbach formed after about 77% crystallization.

The IVA statistics differ from those for main-group pallasites (PMG). Wasson and Choi (2003) reported data on 33 PMG if Phillip's County (for which Ir replicates were dissimilar) is deleted. Of these 33 PMG, 18 have very low Ir contents ($\leqslant$0.1 μg/g) and another eight have low Ir contents ($0.1 < \text{Ir} < 0.32$). Wasson and Choi (2003) interpreted the loci of these low-Ir, high-Au and high-As points to be the result of mixing an evolved liquid either with early crystallized, high-Ir core metal or with refractory mantle metal trapped in the olivine that was introduced into the metallic magma to form the PMG. These interpretations imply roughly 80% crystallization before the olivine-metal mixing event. In contrast, three of the four silica-bearing IVA irons experienced $\leqslant$30% crystallization.

There is an ongoing debate within the iron-meteorite research community between those (like us) who conclude that core crystallization is almost entirely from the center outwards and others (Haack and Scott, 1992, 1993) who hold that cores crystallized almost entirely from the core-mantle interface inwards. A key part of the Haack–Scott argument is that temperatures were lower at the top of the core, and thus that crystallization would have occurred there first. We agree with this view, but we note that, as soon as any solid metal became detached and settled buoyantly to the center of the core, crystallization there would have been far more efficient than crystallization at the edge. An important boundary condition is the temperature gradient across the core. According to Haack and Scott (1992) the total temperature drop across a convecting core with a radius of 10 km is only 0.5 K!

Crystallization of a metallic magma causes an increase in the nonmetal content in a boundary layer immediately adjacent to the solid. Within this boundary layer mixing is by the relatively slow process of diffusion. This enhancement in nonmetal concentration lowers the liquidus temperature. The key difference between crystallization at the top and bottom of the core is that the boundary layer is buoyantly stable at the top of the core and unstable at the bottom. As a result, the mean thickness of this layer is appreciably smaller at the bottom of the core than at the top. Local turbulence would occasionally reduce the thickness of the boundary layer; crystallization then occurred in those regions where the nonmetal concentration happened to become low enough to permit crystallization. Buoyancy causes the bottom of the core to have had much more low-nonmetal surface area than was present at the top of the core. This is the reason that crystallization in the IVA and other magmatic cores occurred at a much higher rate at the bottom of the core.

Fractional crystallization requires continuous, thorough mixing of the residual magma; convection is the only process that can produce the required stirring. Fluid convection is achieved both by crystallization releasing heat and increasing the content of light elements at the bottom of the magma chamber. For a spherical core with radius R that crystallized entirely from the center to the edge we calculate that the three high-Ir silica-bearing IVA irons formed at ~0.67 R and Steinbach at ~0.92 R from the center.

However, it is inevitable that some crystallization also occurred near the core-mantle interface. In fact, Haack and Scott (1992) argued that dendritic crystallization from the core surface downwards accounted for all magmatic irons. Our view is very different. Growth at the top of the core mainly occurs because random convective overturn events sweep away the light-element-enriched layer or because an occasional dendrite manages to protrude through the light-element-rich layer. As discussed above, the rate of crystallization at the top of the core was surely much lower than that at the bottom.

If the mass rate of outwards growth is 100× greater than the downwards rate, then after 99% crystallization, the outer layer of solids would have a thickness of 0.003 R; if R were 20 km, solids produced during 99% crystallization of the core could all occur within an outer layer only 60 m thick. If the core radius were 2 km and 95% of the crystallization occurred from the center outwards, this outer layer preserving 99% of the crystallization would comprise 34 m. We suggest that the metallic portions of high-Ir silica-bearing IVA irons and of the high-Ir pallasites mainly formed in such thin outer zones of the respective cores.

The timing of silicate injection into the core is somewhat constrained by the observation that the (ca. 5-cm) γ-iron crystals in SJN are about 8× smaller than those in silicate-free or tridymite-bearing IVA irons. In Gibeon, Buchwald (1975) observed original γ-iron grains ranging from 10 to 50 cm; a photo of Gibeon in Wasson (1985, Fig. II-7) shows three grains, the largest being 40 cm across. We suggest two possible alternative processes for creating the smaller sizes in SJN: (1) fracturing during the impact event; or (2) that the event occurred before complete growth of the gamma phase, with silicate-rich regions hindering further growth. In any case, it seems clear that the silicates were injected into the core after it had crystallized but before it cooled across the $\gamma/(\alpha+\gamma)$ boundary.

We offer a speculative scenario to account for the mixing of silicates and metal in SJN and Steinbach. We suggest that reduction processes caused SiO_2 to form on orthopyroxene near the core-mantle interface. After the core had largely crystallized, a tectonic event (e.g., mantle collapse or impact) occurred, causing selective melting of materials that were adjacent to silica (and thus could form the opx-silica cotectic). The same event could have caused fractures in the core. The cotectic melt entrained opx from the mantle and opaques from the core as it flowed into these fractures as a slurry. The FeO/(FeO + MgO) ratio of the melt was somewhat higher than in the entrained opx.

As the silicate melt proceeded down the fault conduit into the core, it lost the coarser grains of pyroxene and

as well as many opaques. As a result, the bulk FeO/(FeO + MgO) ratio increased. Thus, the Steinbach (77% crystallization) silicates represent melt/slurry that moved farther and were thus more "evolved."

When the slurry/melt stopped moving, it rapidly lost its heat to the surrounding metal. Orthopyroxene crystallized rapidly, trapping the associated opaques. The opaques had settled out by the time the tridymite crystallized, thus accounting for its dearth of inclusions.

Small amounts of FeS-metal eutectic entrained with the silicate-rich slurry became the last phases to crystallize after the impact-mixing event. Nucleation occurred at metal-silicate boundaries presumably because of the high-surface energy available at this site.

10. Low-Ca clinopyroxene and cooling rates

The occurrence of polysynthetically twinned low-Ca clinopyroxene in Steinbach and São João Nepomuceno has important implications for the origin of IVA irons. Low-Ca clinopyroxene can form in two basic ways: (a) formation from protopyroxene due to quenching from high temperatures, and (b) formation from orthopyroxene by shock. Models involving these two interpretations are outlined below. Because very fast cooling between 1470 and 900 K is required to quench clinopyroxene, an extremely high cooling rate is implied by this interpretation.

10.1. Transformation from protopyroxene after quenching

Low-Ca clinopyroxene is less stable than orthopyroxene at temperatures $\leqslant$1000 K, but it can exist metastably for geologic time at temperatures a few hundred K lower. Low-FeO (Fs < 10 mol%) pyroxene-rich chondrules in unequilibrated chondrites contain polysynthetically twinned low-Ca clinoenstatite formed from protoenstatite after quenching from high temperatures during chondrule formation (e.g., Alexander, 1994). Essentially all type-3 chondrites and many type-4 chondrites contain low-Ca clinopyroxene (Van Schmus and Wood, 1967) formed in this way. However, this phase is absent in type-5 and -6 chondrites because these rocks were metamorphically recrystallized at temperatures above 900 K (Dodd, 1981; Olsen and Bunch, 1984), where low-Ca clinopyroxene is transformed into orthopyroxene (Boyd and England, 1965; Grover, 1972).

10.2. Formation from orthopyroxene by shock

Hornemann and Müller (1971) and Stöffler et al. (1991) found that clinopyroxene lamellae parallel to the (100) planes of parental orthopyroxene grains were formed at shock pressures of ~5 GPa (i.e., corresponding to shock-stage S3). Twinned low-Ca clinopyroxene in unbrecciated type-5 or -6 chondrites (e.g., Fig. 1a of Rubin et al., 1997) is commonly attributed to transformation from orthopyroxene as a result of inhomogeneous shear (i.e., shock). Buseck et al. (1980) noted that, because the twinning process produces two clinoenstatite unit cells from each orthoenstatite unit cell, clinoenstatite formed during shock should have lamellae with widths that are only even multiples of the 0.9-nm unit-cell width of orthopyroxene. They suggested that this provides a means of discriminating between the two mechanisms of formation of low-Ca clinopyroxene.

Haack et al. (1996) studied twinned low-Ca clinopyroxene in Steinbach by transmission electron microscopy (TEM) and found that lamellae widths are both odd and even multiples of the 0.9-nm unit-cell width. Based on the Buseck et al. (1980) arguments, they (and Scott et al., 1996) concluded that the low-Ca clinopyroxene formed from protopyroxene by quenching at 1470 K. The observation that the clinopyroxene lamellae were fractured, as commonly found in chondrules in type-3 chondrites, was cited as additional support for this conclusion.

Because of the importance they attached to the conclusion that the clinopyroxene required quenching from 1470 to 900 K, Scott et al. (1996) maintained that, following their hypothesized reassembly of the asteroid, the temperature of SJN and Steinbach had fallen to ~900 K at a rate of about 10^{12} K/Ma. This inferred increase in cooling rates (by a factor of 10^{10} compared to metallographic cooling rates) was considered to offer support for the impact-scrambling model. Haack et al. (1996) modeled the mean temperature of the reassembled asteroid, and concluded that it was somewhere in the range of 723–973 K; their preferred value appears to be 823 K, estimated for a body with no insulating regolith.

A fact that is not readily explained by the Haack et al. model is why about 80% of the low-Ca pyroxene is orthopyroxene. Because the orthopyroxene and clinopyroxene grains are adjacent, they must have cooled from 1470 to 900 K at the same rate. Why did most of the protopyroxene transform into opx (but not all of it)?

We question whether the chaotic conditions associated with impact-induced shock always produce even spacings in the widths of twin lamellae widths in low-Ca clinopyroxene. Shocks can produce highly variable degrees of heating on small distance scales. For example, dislocations in the target pyroxene followed by metamorphic growth during the high-temperature period that follows the shock could add odd spacings.

It seems plausible that the inferred shock event may have produced small amounts of melt. During cooling the melt would have found itself in the cpx stability field, and the shocked cpx could have served as crystallization nuclei. The resulting mass of cpx would have had both odd and even spacings. We suggest that the best way to show that real shocks always produce even spacings is to determine if only even spacings are found in shocked type-5 and -6 ordinary chondrites. Until such studies have been completed, we suggest that the more plausible (and best working) scenario is that real planetary impacts produce both odd and even spacings.

Rubin et al. (2002) observed large amounts of low-Ca clinopyroxene in the chondritic silicates of the IAB-related iron NWA 468. In these materials the proportion of clinopyroxene corresponds to ~1/3 of the total amount of low-Ca pyroxene. The silicates in this iron meteorite are chondritic and thus were not derived from an igneous melt. The only plausible scenario is that the clinopyroxene in NWA 468 was also produced by impact-induced shock from orthopyroxene since there is no reason to believe that appreciable protopyroxene was ever present. Inversion from protopyroxene requires an implausibly high cooling rate, i.e., 10^{11} times more rapid than that recorded in the IAB Widmanstätten structure.

There is direct evidence of high temperatures produced by late shocks in the IVA asteroid; Ulff-Møller et al. (1995) noted that, in Gibeon and Bishop Canyon, metal adjacent to tridymite had been shock melted.

As discussed in a latter section, the late history of the IVA asteroid is enormously simpler and (we argue) the resulting scenario much more plausible if the low-Ca clinopyroxene formed by shock after the asteroid had cooled to low temperatures, around 500 K.

10.3. Metallographic cooling rate estimates for IVA meteorites

There have been several studies of metallographic cooling rates of IVA iron meteorites. With the exception of constant cooling rates reported by Willis and Wasson (1978) and Yang et al. (1997), all studies have led to wide ranges of cooling rates that correlate with chemical composition. The recent cooling rate estimates of Rasmussen et al. (1995) range from 3400 K/Ma and 1100 K/Ma in Yingde and Bishop Canyon, respectively, down to 19 and 28 K/Ma in Steinbach and Mantos Blancos, respectively. These rates were plotted against log Au in Fig. 6 of Wasson and Richardson (2001) and showed a strong negative correlation. We calculated an F statistic of 18.3 for the 14 points in this array, indicating that the correlation is valid at the >99% confidence level.

As noted by Wasson and Richardson (2001), the cooling rates determined by Yang et al. (1997) in six IVA irons by the cloudy-taenite-island-size method yield similar cooling rates of 28 ± 8 K/Ma with no compositional dependence. It is important to note that this method measures a property established at low temperatures, after the kamacite had completely exsolved from the parental taenite. Thus, it occurred after the hypothetical breakup and scrambling-reassembly event. In fact, the blocking temperature for island-taenite is probably only about 150 K lower than those for the taenite profiles commonly used for metallographic cooling rates.

10.4. Cooling rates and the impact scrambling model

Haack et al. (1996) accepted the validity of the wide apparent range in IVA cooling rates and attempted to explain it by suggesting that, while the core temperature was above about 1120 K (before any of the metal had cooled across the boundary between the γ-field and the $\alpha + \gamma$ field), the parent asteroid experienced a catastrophic breakup event followed by the gravitational reassembly of some fraction of the original asteroidal material. Core fragments ended up at a wide variety of depths as implied by the estimated cooling rates. The resulting scrambled structure was raisin-bread like. The rapid cooling is achieved by mixing cold silicates with the hot (1470 K) core materials. Thus, Steinbach was mixed with silicates having mean temperatures of ~350 K during the postulated scrambling event, and these materials were then buried to the greatest depth observed among IVA irons based on the estimated low cooling rate of Steinbach.

Although this scenario can nominally account for the wide range in cooling rates, a true scrambling cannot account for the correlation of cooling rate with composition. Although Haack et al. (1996) suggested that this correlation is "spurious," resulting from "poor sampling," the strong correlation of cooling rate with Au concentration shows that this view is incorrect. The overall correlation is a fact that must be explained by a successful model even if, as Haack et al. do, one arbitrarily breaks up the IVA group into subsets within which there is no apparent correlation.

To understand more fully the impact-scrambling picture we calculated cooling rates as a function of depth within asteroids. Our results are shown in Fig. 9. In one simulation we used an initial temperature of 825 K and in the other a temperature of 1770 K. We assumed a surface temperature of 200 K, a heat capacity of 837 J $kg^{-1}K^{-1}$ and a thermal conductivity of 2.1 $Wm^{-1}K^{-1}$; both values were taken to be independent of temperature. These thermal parameters are the same as those used by Kunihiro et al. (2004). We did not include an insulating regolith in the model asteroid; addition of a regolith would make it much more difficult to achieve the wide range in cooling rates. Our simulations showed that an asteroid with a radius of 80 km is well suited to explain the lowest cooling-rates estimated by Rasmussen et al. (1995), or the Yang et al. (1997) cooling rate of 28 K/Ma (as evaluated by Wasson and Richardson, 2001). In a body with a porous, insulating outer layer the cooling rates can be achieved in much smaller bodies (our preferred interpretation).

For this hypothetical 80-km asteroid we calculated the depth at which the Rasmussen cooling rates indicated each iron appeared to originate. The relative volume is more useful than depth in assessing how the reassembly model distributes IVA irons. In Fig. 10 the locations of the meteorites are plotted as a histogram showing the distribution in volume space (0 is the center, 1 is the surface of the body). The results are peculiar. If the Rasmussen et al. cooling rates are accepted as correct, then most (9 of 16) of these core fragments ended up in the outermost 20% of the volume (or 7% of the radial depth). One originated

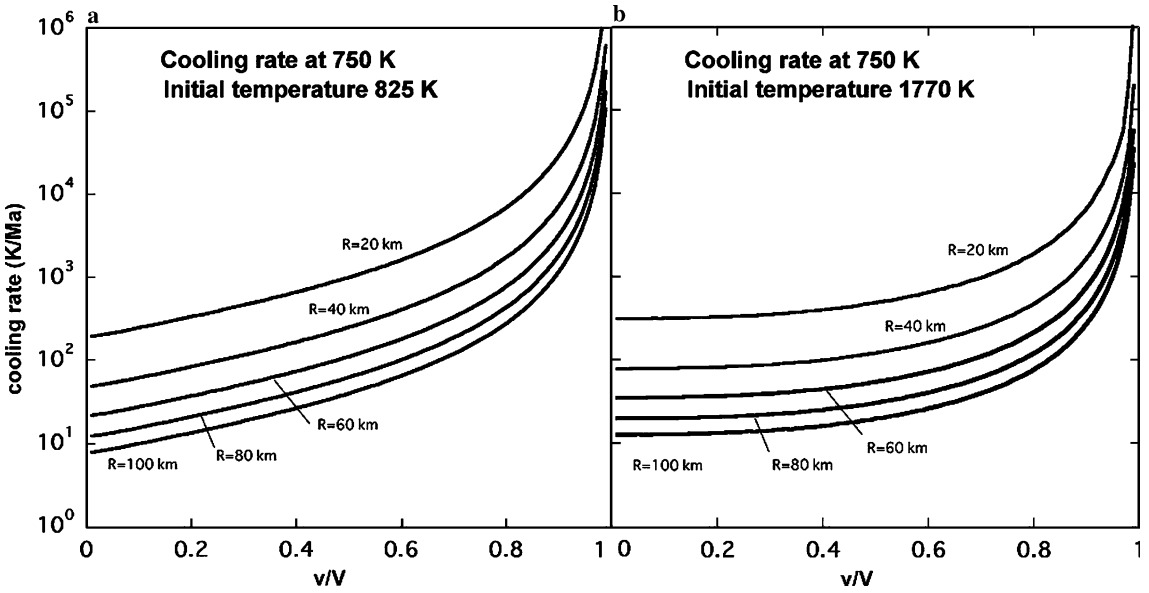

Fig. 9. Calculation of cooling rates as a function of fractional volume within asteroids for two different initial temperatures: (a) 825 K and (b) 1770 K. The following assumptions were made: asteroid surface temperature, 200 K; heat capacity, 837 J $kg^{-1}K^{-1}$; thermal conductivity, 2.1 W $m^{-1}K^{-1}$; no insulating regolith. (The heat capacity and thermal conductivity were assumed to be independent of temperature.)

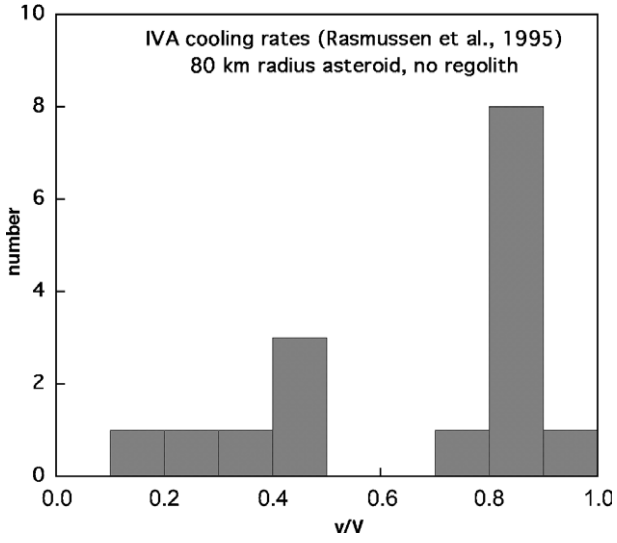

Fig. 10. Histogram showing the numbers of IVA meteorites that formed at different depths based on the cooling-rate estimates of Rasmussen et al. (1995). Depth is represented as volume space wherein 0 is the center and 1 is the asteroid surface. This literal interpretation of the inferred cooling rates implies that most of the original core materials were scrambled upwards into the outer part of the body. As discussed in the text, this is dynamically implausible.

at a slightly greater depth; and the remaining 6 are distributed within the innermost 50% of the asteroidal volume.

11. Distribution of opaque inclusions in silicate grains

The occurrence of opaque inclusions within orthopyroxene but the dearth of such inclusions in tridymite in SJN and Steinbach was first noted by Ulff-Møller et al. (1995). We confirm that observation, and also confirm that the inclusion abundance in SJN pyroxene is an order-of-magnitude greater than that in Steinbach. Ulff-Møller et al. (1995) suggested that this difference could be due to one of three mechanisms (which we expand upon here): (1) increased solubility of sulfide in FeO-rich melts that would crystallize pyroxene instead of more siliceous melts from which tridymite would form; (2) more rapid (earlier) crystallization of pyroxene, rapid enough to trap associated opaque grains, and (3) pushing and concentration of opaques by an advancing pyroxene solidification front. Because pyroxene contains other opaque phases (e.g., chromite, metallic Fe–Ni) in addition to sulfide, mechanism 1 appears, at best, an incomplete explanation. We do not understand mechanism 3, and suspect that there is no such physical mechanism. Mechanism 2 remains viable. We suggest that low-Ca pyroxene was the first liquidus phase, and that it rapidly crystallized on pyroxene crystals entrained in the slurry.

We note that the preferential association of opaque grains with opx is similar to the predominant occurrence of opaque inclusions (mainly oxide grains) within pyroxene in mafic clasts in mesosiderites (Rubin and Mittlefehldt, 1992); mesosiderite plagioclase is relatively free of inclusions. A plausible interpretation is that non-trapped dense opaque inclusions settled out of the melt prior to crystallization of the more-siliceous phase (tridymite in IVA irons, plagioclase in mesosiderites).

Our observations suggest that the inclusion density in low-Ca clinopyroxene is lower than that in the low-Ca orthopyroxene. We suggest that the orthopyroxene crystals with low inclusion densities are preferentially converted to clinopyroxene by shock waves. Perhaps the inclusions cause diffraction in the waves and make it more difficult to achieve uniaxial compression.

12. Late history of the IVA asteroid

By the time the core temperature had dropped to 1400 K most IVA metal had crystallized. Two models of the remaining history of the IVA asteroid have been discussed. (1) In the *traditional (intact core) model* the core cools through the γ field in the Fe–Ni phase diagram, then passes through the $\alpha + \gamma$ field and forms the Widmanstätten pattern. After the body had cooled to low temperatures and negligible further metallurgical changes were occurring, the body was broken up to produce meter-size meteoroids. (2) In the *impact-scrambling model* of Haack et al. (1996), the asteroid (including the core) is fragmented while still in the γ-field (>1250 K) and the core fragments are mixed with mantle materials from all levels; the fragments then fall back together to form the final body, cooling the metal to ~900 K (below the $\gamma/\alpha + \gamma$) boundary.

Our thermal modeling calculations (Fig. 9) revealed that the lowest estimated cooling rates (20–30 K/Ma) observed in IVA irons imply formation in a body with a maximum radius of about 80 km (much smaller if an insulating mega-regolith is added). Wasson (1985) noted that, for an asteroid with a density of 3.5 g cm^{-3}, the escape velocity in m s^{-1} is $1.4 \cdot R$ where R is the asteroidal radius in kilometers. Thus, a IVA-body radius of 80 km yields an escape velocity of ~110 m s^{-1}; a body with a radius of 20 km and an appreciably lower density has an escape velocity of ~20 m s^{-1}. For discussion purposes, we will assume that $R = 80$ km, but most of the arguments are not affected by minor changes in R. In fact, as noted above, the formation of a metallic melt by impact and its draining to the center of the body is more easily achieved in a much smaller asteroid, perhaps 10–20 km in radius.

Our consideration of the mechanics of the Haack et al. (1996) impact-scrambling model provides several reasons for skepticism. Because the cool outer layers of the asteroid should be retained (to provide low post-scrambling metal temperatures), energy limitations associated with the low escape velocity of the asteroid present a major hardship for this model. The relatively low velocities (a mean of 5 km s^{-1}) in the Asteroid Belt create another. At 5 km s^{-1} much of the extra energy required to break up the solid steel core must be obtained by increasing the mass of the projectile.

There are two IVA features that Haack et al. (1996) and Scott et al. (1996) thought were best explained by the impact-scrambling model: (a) the wide range in apparent cooling rates (19–3400 K/Ma, Rasmussen et al., 1995) and the presence of clinopyroxene crystals with odd and even numbered multiples of the unit-cell width, implying formation from protopyroxene by rapid cooling (from 1400 to 800 K in about 3 h). Because of the latter constraint, Haack et al. assumed that the temperature of the IVA core was ca. 1400 K before the impact-scrambling event.

Haack et al. (1996) used simple scaling relationships to discuss the relationship between the specific impact energy and the asteroid diameter. They showed that most of the possible impact outcomes in parameter space involve shattering and dispersal, but they argued that, at slightly lower impact energies, scrambling would result. We agree that launching materials towards all azimuths at suborbital speeds is necessary to achieve scrambling, but we cannot imagine a mechanical basis for expecting this to occur in a single impact event. Haack et al. (1996) did not provide guidance on this point.

We suggest two "Gedankenexperimente" for considering whether it is plausible to mix materials efficiently from the hot core with much-cooler surficial materials: (1) an impact cratering model, and (2) a center-of-core explosion model. According to the Haack et al. (1996) scaling relationships, scrambling a body with a radius of 80 km requires that the radius of the impactor be 0.12 that of the asteroid, or about 10 km. For the model to be successful, it not only needs to produce a large crater in the mantle, it needs to shatter the ductile (1400-K) core and expel the core fragments into space while leaving most of the excavated surficial mantle materials gravitationally bound to the system. This model thus requires the asteroid to be uniformly crushed to fragments having about the same (perhaps 10–100-m) size and that these be accelerated to about the same velocity (slightly less than 110 m s^{-1}). This contrasts with models of cratering events on the surfaces of compact bodies (i.e., the Earth or Moon) in which most of the energy goes into ejecting materials from the crater, with the smallest ejecta reaching the highest velocities (and much of the ejecta achieving velocities > 110 m s^{-1}, the escape velocity on this asteroid).

Even if the bottom of this hypothetical crater reached the core (at a depth of about 0.5 R), we see no reason to expect that appreciable shattering of the core would occur. Instead, we would expect the ductile core to deform but largely remain intact. For this reason we doubt that it is possible to scramble a hot (1400 K) core-bearing asteroid by the impact of a much smaller body (mass 500× smaller than that of the asteroid) at a velocity of 5 km s^{-1}. If it is at all possible to totally disrupt an 80 km asteroid, the impactor would have to be much larger; much of the debris would escape the system, and an appreciable fraction of the final object would be derived from the projectile. We suspect that even such a total disruption would lead to relatively little scrambling of core fragments.

According to our second "Gedankenexperiment," a very large explosion detonated in the center of the IVA core could have disrupted it. But even this highly implausible scenario would not lead to scrambling if the mean velocity imparted to the surficial layer is less than the escape velocity. Instead, we would expect the debris to move radially outwards while largely retaining the relative stratigraphy. Surficial materials would achieve the highest radial velocities. After the fragments reach apoapse and fall back to form a rubble-pile asteroid, the relative depths of individual materials would largely be the same as those in the original asteroid.

As discussed above, we also have serious doubts about the robustness of the constraints that the impact-scrambling model is designed to explain. We argue that IVA cooling rates were probably more-or-less the same, and that the apparent range is an artifact. The strong correlation of the inferred metallographic cooling rates with metal composition implies that a composition-dependent feature affecting the kamacite growth mechanism was not adequately incorporated into the model. As discussed in numerous past papers, cooling rates in a metallic core are determined by conduction through the surrounding mantle, and thus, should be independent of location within the core. We suggest that the prudent course is to accept the near-constant island-taenite cooling rates of Yang et al. (1997) and to assume that future studies will better reveal the details of the kamacite growth mechanism, and lead to a reformulated model that will result in the disappearance of the apparent compositional dependence of the cooling rates. It may be necessary to follow the example of Willis and Wasson (1978) and try a range of phase-diagram boundaries and diffusion-coefficient algorithms (as permitted by data uncertainties) to locate the source of the hypothesized systematic error.

The other feature the impact-scrambling model was designed to explain is the even and odd multiples of the clinopyroxene unit cells; these imply that the clinopyroxene formed during monotonic cooling from high temperatures, but also that the cooling rate between 1400 and 800 K was about 10^{12} K/Ma. We argue above that both odd and even clinopyroxene cell spacings are predicted for impacts that produce large amounts of dislocations and small amounts of shock melt that crystallized clino- or protopyroxene during cooling. The temperature of this melt remained constant as long as latent heat was released, but then dropped quickly thereafter as heat leaked into the cooler surroundings.

Based on this discussion we conclude that the traditional, central-core model (punctuated by at least one late impact event) is the better choice for explaining the properties of the IVA irons. We suggest that future research on the formation of the observed features could usefully be directed towards improving our understanding of the kamacite nucleation and growth, and at investigating the clinopyroxene spacings in heavily shocked type-5 and type-6 chondrites.

13. A simpler model? Formation of IVA from mixed-source precursor materials

The simplest interpretation of the similarity in $\Delta^{17}O$ and $\delta^{18}O$ values between the IVA silicates and the L and LL chondrites is that the IVA silicates formed from L-LL-chondrite precursors. We therefore concluded that this was the first hypothesis to examine, and much of this paper examines how one could create the relatively reduced IVAs with their low contents of volatiles from L-LL chondritic materials that are much more oxidized and have moderate contents of the volatiles S, Ga, and Ge.

We now expand the range of precursor materials to include all kinds of ordinary chondrites including materials intermediate between H and L and treating R chondrites as an anomalous kind of ordinary chondrite. We will also consider the evidence of Choi et al. (1998) regarding the O-isotopic composition of the trapped water in primitive ordinary chondrites.

If the parental materials of IVA silicates were initially as reduced as H chondrites, then much less reduction would be required. It would still be necessary to lose volatiles, and flash evaporation in an open system seems the most suitable for this. But FeS and the nebular carriers of Ga and Ge probably evaporate at lower temperatures than the carriers of the FeO even though the FeO in matrix is accessible to flash evaporation.

How might one plausibly account for the difference in $\Delta^{17}O$ between H-group materials (mean is 0.7‰) and IVA materials (1.2‰). The latter could be achieved if 15% of the O had the $\Delta^{17}O$ value of 4‰ observed in the magnetite of LL3.0 Semarkona by Choi et al. (1998) or if 8% of the O had a $\Delta^{17}O$ value of 7‰, as inferred by Choi et al. (1998) for the water responsible for the formation of the magnetite.

Rubin (2005; see also Wasson, 2000) has shown that there is a correlation between redox state and $\Delta^{17}O$ in the H group; at the oxidized extreme of the group, $\Delta^{17}O$ is about 0.8‰. If we repeat the calculations using this $\Delta^{17}O$ value for the H group, we find that 12.5% of the O would have to come from the exotic source with $\Delta^{17}O = 4.0‰$ or 6.5% from the source with $\Delta^{17}O = 7.0‰$.

The problem is then to find a scenario that would provide both these amounts of exotic oxygen and an environment that would lead to mixing with the other constituents of the magma that produced the IVA silicates. This appears to be challenging.

The great advantage of this kind of model is that it is not necessary to reduce FeO. One must still remove large fractions of volatiles, and the breakdown of FeS would provide the extra Fe metal needed to reduce the Ni concentration down to IVA levels. We argue that this volatile loss is best explained by rapid heating in open systems as provided by impact events.

We will not attempt to assess the relative plausibility of this kind of model relative to the one involving L-LL materials developed above. We consider both of them to be worthy of further exploration.

14. Summary and conclusions

The IVA iron meteorites together with IIAB and IIIAB constitute a trio of large iron meteorite groups that formed by fractional crystallization of slowly cooling cores. Because of the low bulk S content, the initial temperature of the IVA core was higher (~1770 K) than those of the other two groups. At this temperature, all the metal and

nearly all the silicates would have been molten. Thus, the IVA asteroid heat source was strong. The O-isotopic composition of IVA silicates implies that these irons formed from an L-LL-chondrite precursor. The low Ni content of the initial IVA magma requires that the L-LL metal was diluted by metallic Fe. Kunihiro et al. (2004) showed that the low $^{26}Al/^{27}Al$ ratios measured in Semarkona chondrules (Kita et al., 2000) provide too little heat to melt asteroids even if the asteroid accreted immediately after chondrule formation and all of the heat was retained in the interior. Although heat from ^{60}Fe decay may have been able to produce the required extra heat (Mostefaoui et al., 2005), another report (Tachibana and Huss, 2003) reports a much lower $^{60}Fe/^{56}Fe$ initial ratio. Impact heating is therefore suggested as the heat source for the IVA parent body; impact heating has the additional value of producing (in some regions) temperatures high enough to produce metallic Fe by dissociation of FeS and FeO, with the S and O lost from the system as volatiles. High temperatures in an open system could also account for the low Ge/Ni and Ga/Ni ratios in IVA irons; these are 1–2 orders of magnitude lower than those in the presumed L-LL-chondrite precursor.

An additional feature of the IVA meteorites is the unusual nature of their silicates: in two IVA irons the silicate consists of tabular (and probably lamellar) tridymite, in two others mixtures of low-Ca pyroxene and tridymite. The tridymite has few opaque inclusions, whereas such inclusions are abundant in orthopyroxene; inclusions in opx are an order of magnitude more abundant in SJN than in Steinbach. The tabular tridymite has a lower content of minor elements than does the tridymite associated with pyroxene. We argue that SiO_2 veins formed by vapor deposition in cracks in the solid ($T < 1600$ K) IVA core; we can find no other mechanism to account for the petrographic evidence. Because SiO_2 has a very low vapor pressure, we propose that Si was transported as SiO(g). The reducing agent may have been C or Si dissolved in the core. It is possible that some of the SiO_2 present in the pyroxene-silica assemblages was also formed as a vapor deposit.

We propose that the IVA silicates were emplaced as a shock-produced slurry, with the melt composition being close to the pyroxene–silica cotectic (as first suggested by Ulff-Møller et al., 1995). The shock pressure forced part of the slurry through cracks in the core; as it progressed it lost pyroxene and opaque phases and gradually became more ferroan. We thus interpret the Steinbach silicates to be more evolved than those in SJN, consistent with the greater depth associated with the more-evolved metal in Steinbach.

The low-Ca clinopyroxene in SJN and Steinbach may have formed by a later shock that produced low-Ca clinopyroxene and a minor amount of melt. Although shocking massive orthopyroxene leads to a doubling of the number of crystals (and thus lattice spacings that form multiples of two), even the tiniest amount of clinopyroxene growth associated with annealing dislocations or crystallization of melt would have added odd numbers to the multiples of the lattice spacings.

Haack et al. (1996) proposed that the wide inferred range (3400–19 K/Ma, according to Rasmussen et al., 1995) of IVA metallographic cooling rates was best understood by an impact-scrambling model. Because the cooling rate data strongly correlate with metal composition, an alternative would seem to be composition-dependent effects in the α-iron-formation mechanism that are not adequately included in current nucleation and growth models. A more recent report based on the island size in cloudy taenite (Yang et al., 1997) found no evidence of cooling-rate variations in group IVA. We therefore conclude that the preferred model of group-IVA formation is the traditional monotonic cooling model followed by an impact event that converted some orthopyroxene into clinopyroxene.

Acknowledgments

This research was greatly enhanced by the generous loan of the large SJN specimen by Elizabeth Zucolotto of the Brazilian National Museum in Rio de Janeiro. We are also grateful to T. McCoy and L. Welzenbach of the Smithsonian Institution for the loan of thin and thick sections of SJN and to G. Kurat for permission to use a photograph of a silica-bearing Gibeon specimen. We thank E. Scott and K. Rasmussen for help in tracking down a missing section of Gibeon, Frank Wlotzka and Jutta Zipfel for help in searching for images and for silica-bearing Gibeon specimens. We appreciate helpful comments from A. J. Brearley and detailed and helpful reviews by H. Haack, D. Lauretta, H.J. Melosh, A. Ruzicka, and D.W. Mittlefehldt. YM thanks H. Yurimoto for partial financial support and the opportunity to come to UCLA. This research was supported mainly by NASA Grant NAG5-12058 (JTW). Additional support was provided by NASA Grant NAG5-4766 (AER).

Associate editor: David W. Mittlefehldt

References

Alexander, C.M.O., 1994. Trace element distributions within ordinary chondrite chondrules: implications for chondrule formation conditions and precursors. *Geochim. Cosmochim. Acta* **58**, 3451–3467.

Berman, R.G., 1988. Internally-consistent thermodynamic data for minerals in the system Na_2O–K_2O–CaO–MgO–FeO–Fe_2O_3–Al_2O_3–SiO_2–TiO_2–H_2O–CO_2. *J. Petrol.* **29**, 445–522.

Berwerth, F., 1902. Der Meteoreisenzwilling von Mukerop, Bezirk Gibeon, Deutsch-Südwest-Afrika. Sitzungsber. *Akad. Wiss.* **11** (Serie I), 646–667.

Bizzarro, M., Baker, J.A., Haack, H., 2004. Mg isotope evidence for contemporaneous formation of chondrules and refractory inclusions. *Nature* **431**, 275–278.

Boyd, F.R., England, J.L., 1965. The rhombic enstatite–clinoenstatite inversion. *Carnegie Inst. Washington, Ann. Rpt. Dir. Geophys. Lab.* **1964–65**, 117–120.

Brandes, E.A., Brook, G.B., 1992. *Smithells Metal Reference Book*. Butterworth-Heinemann, CA, p. 1600.

Buchwald, V.F., 1975. *Handbook of Iron Meteorites*. University of California Press, Berkeley, CA, p. 1418.

Buseck, P.R., Nord, G.L., Veblen, D.R., 1980. Subsolidus phenomena in pyroxenes. *Rev. Mineral.* **7**, 117–211.

Chabot, N.L., 2004. Sulfur contents of the parental metallic cores of magmatic iron meteorites. *Geochim. Cosmochim. Acta* **68**, 3607–3618.

Chabot, N.L., Jones, J.H., 2003. The parameterization of solid metal–liquid metal partitioning of siderophile elements. *Meteorit. Planet Sci.* **38**, 1425–1436.

Choi, B.-G., McKeegan, K.D., Krot, A.N., Wasson, J.T., 1998. Extreme oxygen-isotope compositions in magnetite from unequilibrated ordinary chondrites. *Nature* **392**, 577–579.

Clayton, R.N., Mayeda, T.K., 1996. Oxygen isotope studies of achondrites. *Geochim. Cosmochim. Acta* **60**, 1999–2017.

Dodd, R.T., 1981. *Meteorites—A Petrologic-Chemical Synthesis*. Cambridge, New York, p. 368.

Grossman, J.N., Brearley, A.J., 2005. The onset of metamorphism in ordinary and carbonaceous chondrites. *Meteorit. Planet Sci.* **40**, 87–122.

Grover, J.E., 1972. The stability of low-clinoenstatite in the system $Mg_2Si_2O_6$–$CaMgSi_2O_6$ (abstract). *Trans. Am. Geophys. Union* **53**, 539.

Haack, H., Scott, E.R.D., 1992. Asteroid core crystallization by inward dendritic growth. *J. Geophys. Res.* **97**, 14727–14734.

Haack, H., Scott, E.R.D., 1993. Chemical fractionations in group IIIAB iron meteorites: origin by dendritic crystallization of an asteroidal core. *Geochim. Cosmochim. Acta* **57**, 3457–3472.

Haack, H., Scott, E.R.D., Love, S.G., Brearley, A., 1996. Thermal histories of IVA stony-iron and iron meteorites: evidence for asteroid fragmentation and reaccretion. *Geochim. Cosmochim. Acta* **60**, 3103–3113.

Hornemann, U., Müller, W.F., 1971. Shock-induced deformation twins in clinopyroxene. *N. Jb. Mineral* **6**, 247–256.

JANAF, 1998. Thermochemical Tables. American Chemical Society, p. 1951.

Jarosewich, E., 1990. Chemical analyses of meteorites: a compilation of stony and iron meteorite analyses. *Meteoritics* **25**, 323–337.

Jones, R.H., 1990. Petrology and mineralogy of type II, FeO-rich chondrules in Semarkona (LL3.0): origin by closed-system fractional crystallization, with evidence for supercooling. *Geochim. Cosmochim. Acta* **54**, 1785–1802.

Jones, J.H., Malvin, D.J., 1990. A nonmetal interaction model for the segregation of trace metals during solidification of Fe–Ni–S, Fe–Ni–P, and Fe–Ni–S–P alloys. *Metall. Trans.* **21b**, 697–706.

Kallemeyn, G.W., Rubin, A.E., Wang, D., Wasson, J.T., 1989. Ordinary chondrites: bulk compositions, classification, lithophile-element fractionations, and composition-petrographic type relationships. *Geochim. Cosmochim. Acta* **53**, 2747–2767.

Keil, K., Stöffler, D., Love, S.G., Scott, E.R.D., 1997. Constraints on the role of impact heating and melting in asteroids. *Meteorit. Planet Sci.* **32**, 349–363.

Kita, N.T., Nagahara, H., Togashi, S., Morishita, Y., 2000. A short duration of chondrule formation in the solar nebula: evidence from ^{26}Al in Semarkona ferromagnesian chondrules. *Geochim. Cosmochim. Acta* **64**, 3913–3922.

Kleine, T., Mezger, K., Palme, H., Scherer, E., Munker, C., 2005. Early core formation in asteroids and late accretion of chondrite parent bodies: evidence from ^{182}Hf–^{182}W in CAIs, metal-rich chondrites and iron meteorites. *Geochim. Cosmochim. Acta* **69**, 5805–5818.

Kunihiro, T., Rubin, A.E., McKeegan, K., Wasson, J.T., 2004. Initial ^{26}Al/^{27}Al in carbonaceous–chondrite chondrules: too little ^{26}Al to melt asteroids. *Geochim. Cosmochim. Acta* **68**, 2947–2957.

Melosh, H.J., 1989. *Impact Cratering: A Geologic Process*. Oxford University Press, New York, p. 245.

Moore, C.B., Lewis, C.F., Nava, D., 1969b. Superior analyses of iron meteorites. In: Millman, P.M. (Ed.), *Meteorite Research*. Reidel, pp. 738–748.

Mostefaoui, S., Lugmair, G.W., Hoppe, P., 2005. ^{60}Fe: a heat source for planetary differentiation from a nearby supernova explosion. *Astrophys. J.* **625**, 271–277.

Olsen, E.J., Bunch, T.E., 1984. Equilibration temperatures of the ordinary chondrites: a new evaluation. *Geochim. Cosmochim. Acta* **48**, 1363–1365.

Rasmussen, K.L., Ulff-Møller, F., Haack, H., 1995. The thermal evolution of IVA iron meteorites: evidence from metallographic cooling rates. *Geochim. Cosmochim. Acta* **59**, 3049–3059.

Robie, R.A., Hemingway, B.S., Fisher, J.R., 1978. Thermodynamic Properties of Minerals and Related Substances at 298.15 K and 1 Bar (10^5 Pascals) Pressure and at Higher Temperatures. U.S. Geol. Survey Bull. 1452, U.S. Govt. Printing Office, Washington, p. 456.

Roeder, P.L., Emslie, R.F., 1970. Olivine-liquid equilibrium. *Contrib. Mineral Petrol.* **29**, 275–289.

Rubin, A.E., 2005. Relationships among intrinsic properties of ordinary chondrites: oxidation state, bulk chemistry, oxygen-isotopic composition, petrologic type and chondrule size. *Geochim. Cosmochim. Acta* **69**, 4907–4918.

Rubin, A.E., Mittlefehldt, D.W., 1992. Classification of mafic clasts from mesosiderites: implications for endogenous igneous processes. *Geochim. Cosmochim. Acta* **56**, 827–840.

Rubin, A.E., Scott, E.R.D., Keil, K., 1997. Shock metamorphism of enstatite chondrites. *Geochim. Cosmochim. Acta* **61**, 847–858.

Rubin, .E., Ulff-Møller, F., Wasson, J.T., Carlson, W.D., 2001. The Portales Valley meteorite breccia: evidence for impact-induced melting and metamorphism of an ordinary chondrite. *Geochim. Cosmochim. Acta* **65**, 323–342.

Rubin, A.E., Kallemeyn, G.W., Wasson, J.T., 2002. A IAB-complex iron meteorite containing low-Ca clinopyroxene: Northwest Africa 468 and its relationship to lodranites and formation by impact melting. *Geochim. Cosmochim. Acta* **66**, 3657–3671.

Schaudy, R., Wasson, J.T., Buchwald, V.F., 1972. The chemical classification of iron meteorites-VI.A reinvestigation of irons with Ge concentrations lower than 1 ppm. *Icarus* **17**, 174–192.

Scott, E.R.D., Haack, H., McCoy, T., 1996. Core crystallization and silicate-metal mixing in the parent body of the IVA iron and stony-iron meteorites. *Geochim. Cosmochim. Acta* **60**, 1615–1631.

Sonett, C.P., Colburn, D.S., Schwartz, K., Keil, K., 1970. The melting of asteroidal-sized bodies by unipolar dynamo induction from a primordial T Tauri sun. *Astrophys. Space Phys.* **7**, 446–488.

Stöffler, D., Keil, K., Scott, E.R.D., 1991. Shock metamorphism of ordinary chondrites. *Geochim. Cosmochim. Acta* **55**, 3845–3867.

Tachibana, S., Huss, G.R., 2003. The initial abundance of ^{60}Fe in the solar system. *Astrophys. J.* **588**, L41–L44.

Taylor, G.J., Keil, K., McCoy, T., Haack, H., Scott, E.R.D., 1993. Asteroid differentiation: pyroclastic volcanism to magma oceans. *Meteoritics* **28**, 34–52.

Ulff-Møller, F., Rasmussen, K., Prinz, M., Palme, H., Spettel, B., Kallemeyn, G., 1995. Magmatic activity on the IVA parent body: evidence from silicate-bearing iron meteorites. *Geochim. Cosmochim. Acta* **59**, 4713–4728.

Van Schmus, W.R., Wood, J.A., 1967. A chemical-petrologic classification for the chondritic meteorites. *Geochim. Cosmochim. Acta* **31**, 747–765.

Wang, J., Davis, A.M., Clayton, R.N., Mayeda, T.K., Hashimoto, A., 2001. Chemical and isotopic fractionation during the evaporation of the FeO–MgO–SiO_2–CaO–Al_2O_3–TiO_2 rare earth element melt system. *Geochim. Cosmochim. Acta* **65**, 479–494.

Wang, P.-L., Rumble III, D., McCoy, T.J., 2004. Oxygen isotopic compositions of IVA iron meteorites: implications for the thermal evolution derived from in situ ultraviolet laser microprobe analyses. *Geochim. Cosmochim. Acta* **68**, 1159–1171.

Warren, P.H., 1986. The bulk-Moon MgO/FeO ratio: a highlands perspective. In: Hartmann, W.K., Phillips, R.J., Taylor, G.J. (Eds.), *Origin of the Moon*. Lunar and Planetary Institute, pp. 279–310.

Wasson, J.T., 1972. Parent-body models for the formation of iron meteorites. *Proc. Internat. Geol. Cong.* **24** (15), 161–168.

Wasson, J.T., 1985. *Meteorites: Their Record of Early Solar System History*. Freeman, p. 267.

Wasson, J.T., 1996. Chondrule formation: energetics and length scales. In: Hewins, R.H., Jones, R., Scott, E.R.D. (Eds.), *Chondrules and the Protoplanetary Disk*. Cambridge University, Cambridge, pp. 45–51.

Wasson, J.T., 1999. Trapped melt in IIIAB irons; solid/liquid elemental partitioning during the fractionation of the IIIAB magma. *Geochim. Cosmochim. Acta* **63**, 2875–2889.

Wasson, J.T., 2000. Oxygen-isotopic evolution of the solar nebula. *Rev. Geophys.* **38**, 491–512.

Wasson, J.T., Choi, B.-G., 2003. Main-group pallasites—chemical composition, relationship to IIIAB irons, origin. *Geochim. Cosmochim. Acta* **67**, 3079–3096.

Wasson, J.T., Kallemeyn, G.W., 1988. Compositions of chondrites. *Philos. Trans. R. Soc. London* **A325**, 535–544.

Wasson, J.T., Kallemeyn, G.W., 2002. The IAB iron–meteorite complex: a group, five subgroups, numerous grouplets, closely related, mainly formed by crystal segregation in rapidly cooling melts. *Geochim. Cosmochim. Acta* **66**, 2445–2473.

Wasson, J.T., Richardson, J.W., 2001. Fractionation trends among IVA iron meteorites: contrasts with IIIAB trends. *Geochim. Cosmochim. Acta* **65**, 951–970.

Wasson, J.T., Trigo-Rodriguez, J.M., 2004. Evaporation during chondrule formation, recondensation as fine particles, and the condensation of S and other volatile elements (abstract). *Lunar Planet Sci.* **35**, 2140.

Willis, J., Wasson, J.T., 1978. Cooling rates of group IVA iron meteorites. *Earth Planet Sci. Lett.* **40**, 141–150.

Yang, C.-W., Williams, D.B., Goldstein, J.I., 1997. A new empirical cooling rate indicator for meteorites based on the size of the cloudy zone of the metallic phases. *Meteorit. Planet Sci.* **32**, 423–429.